Bubble Clouds and Langmuir Circulation: Observations and Models

S. A. THORPE

SOES, Southampton Oceanography Centre, Southampton, United Kingdom

T. R. OSBORN

Department of Earth and Planetary Science, The Johns Hopkins University, Baltimore, Maryland

D. M. FARMER

Graduate School of Oceanography, University of Rhode Island, Narragansett, Rhode Island

S. VAGLE

Institute of Ocean Sciences, Patricia Bay, Sidney, British Columbia, Canada

(Manuscript received 16 October 2002, in final form 3 February 2003)

ABSTRACT

Concurrent measurements of the rate of dissipation of turbulent kinetic energy and the void fraction and size distribution of near-surface bubbles are described. Relatively high dissipation rates and void fractions are found in bubble bands produced by Langmuir circulation. The mean dissipation rates observed in the bands are close to those at which the dynamics of algae is significantly affected. The data are used to test basic assumptions underpinning models of subsurface bubbles and associated air–sea gas transfer. A simple model is used to examine the qualitative effect of Langmuir circulation on the vertical diffusion of bubbles and the representation of Langmuir circulation in models of gas transfer. The circulation is particularly effective in vertical bubble transfer when bubbles are injected by breaking waves to depths at which they are carried downward by the circulation against their tendency to rise. The estimated value of the ratio r of the eddy diffusivity of particles (resembling bubbles) K_p to the eddy viscosity K_z depends on depth z and on the form selected for K_z. The effects of nonoverlapping or superimposed Langmuir cells of different size may be very different. Multiple nonoverlapping cells of similar scales with K_z independent of depth can result in concentration profiles that resemble those of a law-of-the-wall K_z. It is demonstrated that model prediction of bubble distributions and of gas transfer (which is related to bubble submergence time) is sensitive to K_z and to the size distribution of Langmuir circulation cells.

1. Introduction

The subsurface bubble clouds produced by breaking waves are a powerful and persuasive indicator of the presence of processes of transport from the atmosphere to the upper ocean. They are important in near-surface optics (Stramski and Tegowski 2001; Terrill et al. 2001), acoustic propagation and ambient noise in the sea (Farmer and Lemon 1984) and particularly in air–sea gas flux. It is known from observations—for example, those reported by Thorpe and Hall (1983), Thorpe (1984c), Farmer and Li (1995), and Thorpe et al. (2003)—that bubble bands form within the downwelling regions produced by Langmuir circulation (hereinafter referred to as Lc). Zedel and Farmer (1991) demonstrate that the most intense and deepest-going bubble clouds appear within these bands, while Thorpe et al. (2003) show that the rate of dissipation of turbulent kinetic energy per unit mass ε is, on average, enhanced within the bands. There has, however, been no simultaneous measurements reported of ε and bubble void fraction or size distribution. Such measurements made using an autonomous underwater vehicle (AUV), Autosub, are described in section 2.

Bubbles form an important route for air–sea gas transfer but, as explained in section 3, models are presently required to assess the transfer rates. Several assumptions concerning bubbles and their dynamics are commonly made in devising these models. Their validity is tested in section 4 using the data described in section 2. As explained in section 5, it is usual for the models to represent the dispersive effects of small-scale turbulence by a constant eddy diffusivity coefficient and to adopt

Corresponding author address: Dr. S. A. Thorpe, Bodfryn, Glanrafon, Llangoed, Anglesey LL58 8PH, United Kingdom.
E-mail: oss413@sos.bangor.ak.uk

a simple ''one cell size'' representation of Lc. These aspects of the models are examined at length in sections 7–9, in particular the effects of Lc in promoting vertical diffusion and the effects of including a representation of the commonly observed hierarchy of cell sizes.

2. Observations of bubbles and Lc

Concurrent measurements of the rate of dissipation of turbulent kinetic energy per unit mass ε, void fractions v_f, and bubble size distributions have been made using the AUV Autosub running along constant depth ''legs'' around a 5 km square at depths of 1.5–15 times the significant wave height H_s. Measurements described below are in fairly steady winds of about 11.5 m s^{-1} with a fetch of 20 km and wave ages of 11.7–17.2. The location, the environmental conditions, and the methods used to determine ε are described by Thorpe et al. (2003, mission1). Turbulence is measured from shear probes mounted on the front of the vehicle, and void fraction v_f and bubble size distribution are measured from a bubble resonator (Farmer et al. 1998) mounted on top of the AUV. Estimates of ε and v_f are generally made at 1-s intervals. The void fraction v_f is measured 0.6 m above and 5.84 m behind the turbulence sensors. In Figs. 1–3, the horizontal offset is corrected from the time record using the mean AUV speed through the water of 1.25 m s^{-1} and the turbulence probe depth is used to specify depth z. Individual estimates of void fractions and bubble size distributions have a random uncertainty of a factor of about 2 but a mean calibration uncertainty of 10%–20%. Owing to interference between the AUV's ADCP and the resonator, the threshold of reliable estimates of v_f is 10^{-8} and of bubble radii is about 25 μm.

It is found in laboratory experiments that as much as 40% of the energy lost by breakers may go into the production of bubble clouds (Lamarre and Melville 1991, 1994). Some 90% of the turbulent energy generated is dissipated within four wave periods after breaking whilst it penetrates to depths of $(1.25 \pm 0.25)H$ for spilling breakers or $(1.75 \pm 0.45)H$ for plunging breakers. Here H is the height of the breaking wave (Rapp and Melville 1990). (Rotors formed in wave breaking and which may trap bubbles, reach only to depths of about H, Melville et al. 2002). Breaker heights observed at sea are typically 30% less than the significant wave height H_s (Gemmrich and Farmer 1999b) so that the direct injection of turbulence by even plunging breakers reaches depths of no more than about $1.5H_s$. Although in the laboratory experiments waves break in a static fluid without the preexisting turbulence that is present in the upper ocean, these results suggest that the Autosub observations are beyond the direct influence of the breaking waves and that bubbles are carried to the operational depth by turbulent diffusion or by advection in Lc rather than by the downward jetlike flow induced by the falling crest of plunging breakers.

This conclusion is supported by the finding that the mean rate of turbulent dissipation measured from Autosub is consistent with the law of the wall relation, $\varepsilon = u_{*w}^3/kz$ (Thorpe et al. 2003). Here z is the distance below the mean water surface, k is von Kármán's constant (about 0.41), and u_{*w} is the friction velocity in the water. The distribution of ε is lognormal and the majority of the highest dissipation rates in the range $1.5 < z/H_s < 6$ are where there is a significant void fraction and therefore bubbles. This is shown in Fig. 1 at depths $z/H_s =$ (top) 2.22 and (bottom) 4.16. Two histograms (pdfs) are shown at each depth to the left of the figure. The upper is that of ε, and the lower (black) is that of ε when $v_f > 2 \times 10^{-8}$, an arbitrary value taken as twice the threshold of reliable estimates, selected as a well-defined level of v_f that indicates the presence of bubble clouds. The ratios of the number of values of ε found in bubble clouds to those in the full record are shown on the right and increase with increasing ε. Mean dissipation rates in bubble clouds at $z/H_s = 2.22$ exceeds the total record average dissipation rates by factors of 0.57, 0.83, 0.98, and 1.22 when $v_f > 10^{-8}$, 2×10^{-8}, 5×10^{-8}, and 10^{-7}, respectively. Equivalent values at $z/H_s = 4.16$ are 1.03, 1.18, and 1.39 when $v_f > 10^{-8}$, 2×10^{-8} and 5×10^{-8}, respectively. The observations imply that the greatest dissipation rates are found in the most intense clouds and that, when considering the effect of turbulence on bubble dynamics, it is not appropriate to take mean values of ε but rather the larger values that represent those within bubble clouds.

The largest values of ε at this depth are $\varepsilon_{\max} \approx 3.2 \times 10^{-5}$ m^2 s^{-3} and the greatest value of v_f is $v_{f\max} \approx 2.5 \times 10^{-6}$. The pdf of v_f measured at $W_{10} = 11.6$ m s^{-1} decreases steadily as v_f increases from its threshold value of 10^{-8}. At 2.2-m depth, 5% of the full record of 28 204 values exceed 8.1×10^{-8} and 1% exceed 2.8×10^{-7}. Corresponding 5% and 1% values for a record with 28 084 values at 4.2 m are 2.4×10^{-8} and 6.2×10^{-8}, respectively.

Much larger instantaneous values of v_f are found at shallower depths shortly after waves have broken (Lamarre and Melville 1991; Farmer and Gemmrich 1996). The mean v_f decreases approximately exponentially with depth with decay scales of order 1 m (Farmer et al. 1998). Mean values of v_f measured at $z/H_s = 2.24$ at the location of bubble clouds left by breaking waves show a gradual increase in time of about 14% between 30 and 70 s after wave breaking, presumably as a consequence of vertical dispersion and advection of bubbles in Lc. This rise in v_f accompanies the 50% increase in ε between about 30 and 50 s after breaking, followed by a reduction over the next 20 s, reported by Thorpe et al. (2003).

The related mean horizontal structure of ε and v_f are shown in Fig. 2, conditionally sampled average sections of ε and log(mean v_f) across (Fig. 2a) bubble clouds (regions where $v_f > 2 \times 10^{-8}$) at a depth of 4.04 m

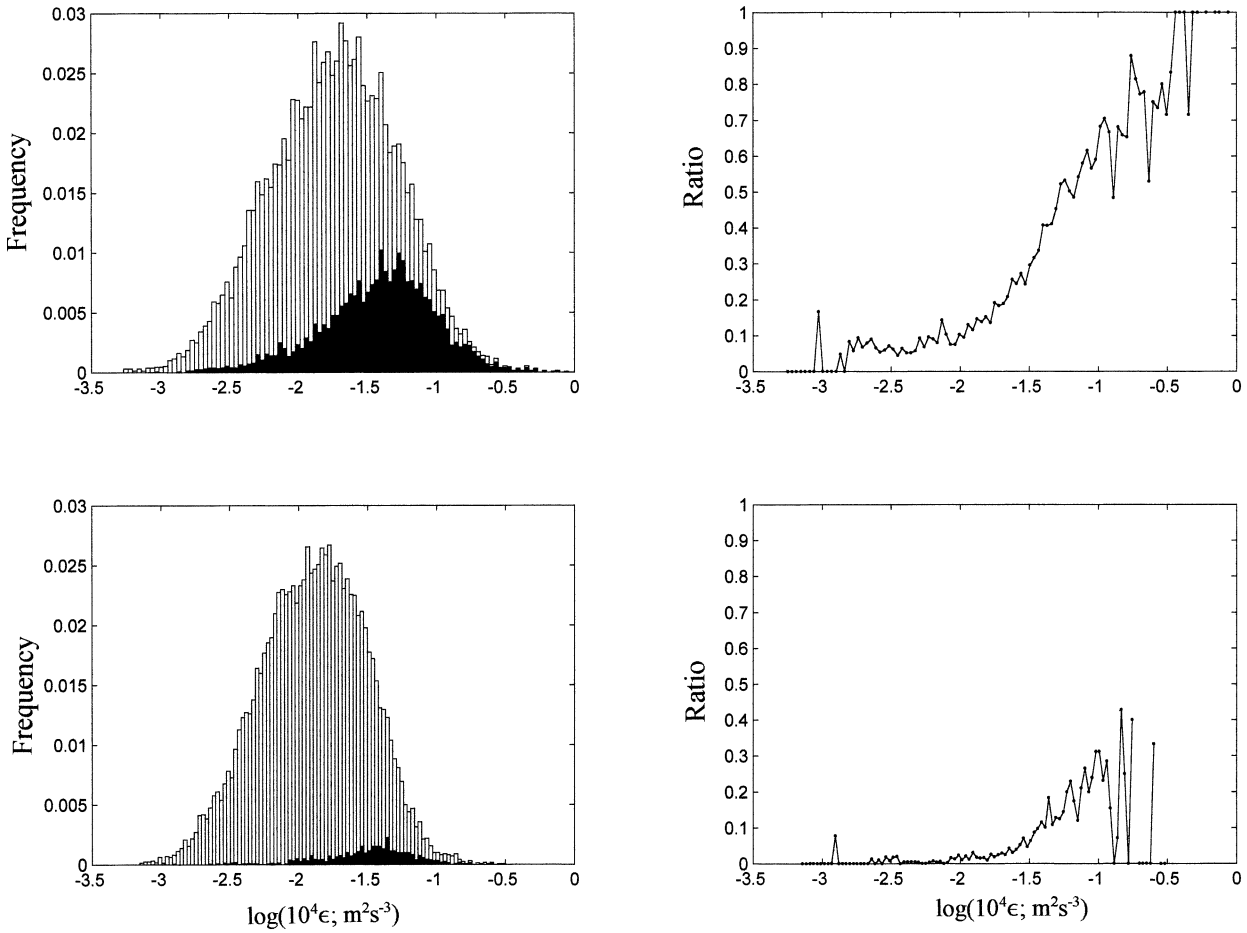

FIG. 1. Histograms of dissipation. On the right are the normalized histograms (pdfs) of logε at mean depths z of (top) 2.22 m (z/H_s = 2.2, W_{10} = 10.8 m s^{-1}) and (bottom) 4.16 m (z/H_s = 4.16, W_{10} = 11.7 m s^{-1}). The regions in black show the proportion of dissipation rates that are found in regions of bubble clouds where the void fraction $v_f > 2 \times 10^{-8}$. The corresponding ratios of logε values in bubble clouds to those in the full record are shown on the left.

(z/H_s = 4.21) and (Fig. 2b) Lc bubble bands at two depths, 2.1 m (z/H_s = 1.92) and (Fig. 2c) 3.9 m (z/H_s = 4.35).[1] The wind speeds in Figs. 2a–c are 11.7, 10.6, and 11.9 m s^{-1}, respectively. Higher than average values of ε and v_f are observed near the centre of the bubble clouds or the bands which are located at time t = 0. Vertical displacements of the Autosub indicate mean downward motions of typically 0.5 cm s^{-1} in bubble clouds and 2–6 cm s^{-1} in Lc bands. It appears that, as argued by Zedel and Farmer (1991), most, if not all, the bubble clouds at the observed depths are a consequence of downwelling in Lc. Because of the variable nature of Lc and the broken cloud structure within the bands (resulting partly from the intermittent supply of bubbles from the random field of breakers), it is probable that many of the clouds contributing to Fig. 2a are not recognized as Lc bands even by the rigorous method of objective identification.

Figure 3 shows bubble size distributions at the center of 30 Lc bands at (top) 2.1 m and (bottom) 3.9 m. Figure 3a shows the bubble number concentration, $n(a)da$ (the number of bubbles per cubic meter with radii between $a - 0.5$ μm and $a + 0.5$ μm) averaged at the centers of all the bands at (top) 2.1- and (bottom) 3.9-m depth. For comparison, the dashed line shows the much smaller bubble concentrations at $\pm$10 m from the center of the bands. Concentrations are smaller at greater depth. At the shallower depth there appears to be a peak at a radius of about 30 μm with corresponding concentrations of 1.8×10^4 bubbles/1-μm radius band/cubic meter. Figure 3b shows log($a^3n(a)da$), where $a^3n(a)da$ is proportional to the void fraction per unit radius band averaged over

[1] Details of conditional sampling and of the variation of other measured quantities are given by Thorpe et al. (2003). In brief, the conditional plots consist of sets of values which are averaged together so as to provide a representation of the mean variation across a time location identified by some criterion, here the time of crossing the centre of bubble clouds or bands of bubbles associated with Lc. Bands are identified using a forward and a sideways pointing side-scan sonar carried on Autosub. The forward pointing sonar identifies bands as they are approached, and the sideways pointing sonar views bands as the AUV converges on them. Crossing times are determined by objective analysis.

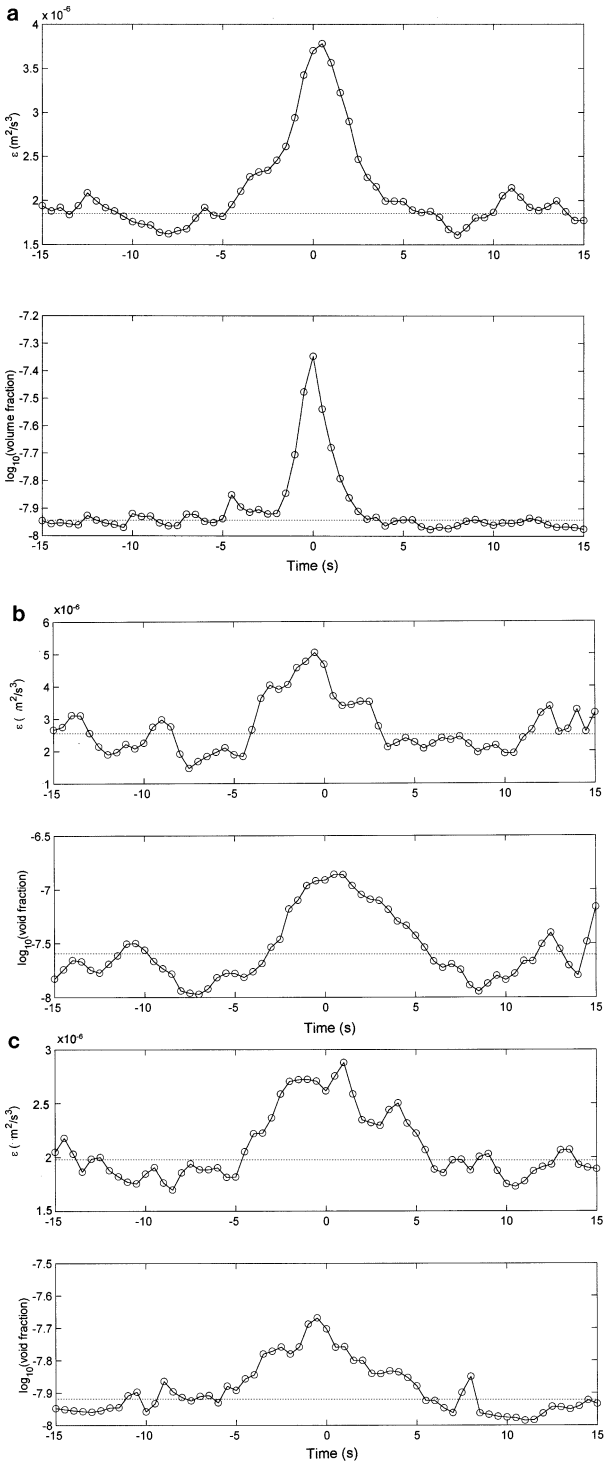

FIG. 2. Conditional sample plots made by taking averages across (a) 196 bubble clouds (regions where $v_f > 2 \times 10^{-8}$) at a depth of 4.04 m ($z/H_s = 4.21$, $W_{10} = 11.8$ m s^{-1}), (b) 31 Langmuir bubble bands at a depth of 2.1 m ($z/H_s = 1.92$, $W_{10} = 10.6$ m s^{-1}), and (c) 154 bands at a depth of 3.9 m ($z/H_s = 4.35$, $W_{10} = 11.9$ m s^{-1}), showing the variation of dissipation ε (m^2 s^{-3}) and void fraction $\log(v_f)$. The bands were crossed at approximately 45° (see Thorpe et al. 2003) and a time of 10 s corresponds to a distance of about 12.5 m. Dashed horizontal lines show leg-mean values.

the Lc bands, with the dashed lines showing values at ±10 m for reference. Bubbles contributing most to the void fraction are of small radii, mostly less than about 160 μm. It is found by plotting separate curves of $\log[a^3 n(a) da]$ versus a at the center of Lc bands that the radius at which the void fraction is greatest decreases as the overall void fraction decreases. This is consistent with Lc cells that have larger vertical downwelling speeds carrying more large bubbles and a consequently producing a greater void fraction.

3. Models of gas flux and Lc

Bubbles transfer their constituent gases into the water by dissolution. For some gases at high enough wind speeds (typically those exceeding the global ocean average surface wind speed of about 7.8 m s^{-1}), bubbles appear to provide an efficient and possibly dominant mechanism of air–sea gas transfer (Woolf and Thorpe 1991; Schudlich and Emerson 1996) although, largely because of the existing uncertainty in quantifying their effect and relating it to forcing factors (e.g., wind speed), this route of gas transfer is not always represented in basinwide or global estimates of air–sea gas flux (e.g., see Garcia and Keeling 2001). While it is now possible to measure the bubble size distribution in breakers (Deane and Stokes 2002) and as a function of depth below the sea surface (Farmer et al. 1998, 1999), this information about bubbles is insufficient to allow the direct estimation of their gas transfer into the surrounding water, even when supplemented by measures of the gas saturation in the bubble-containing water. In being diffused downward from the sea surface by turbulent motions, including Lc, the gases within bubbles pass into solution at rates that depend on the individual gases, their partial pressures in bubbles and their saturation within the surrounding water, as well as on the bubble radii and on the degree to which the surface of bubbles may be covered by surfactants. Consequently, at depth, the relative concentration of gases within bubbles is no longer that in the air above the ocean from which they originated. The mean partial pressures of the gases within bubbles are unknown and it is not yet possible to measure them at sea. The gas flux cannot therefore be estimated directly from observations. Unless or until measurements of gas composition of bubbles in the sea becomes feasible or laboratory experiments can be conducted that fully represent the wave breaking and the bubble and turbulence production that occurs at sea, resort must be made to the use of models of bubble transport and dissolution, constrained by available measurements, to estimate the in situ gas composition of bubbles and hence the bubble contribution to air–sea gas flux.

A variety of dynamical models have been devised to estimate the gas flux from bubbles created by breaking waves. Models include the compression of bubbles, the dissolution of their component gases as they are sub-

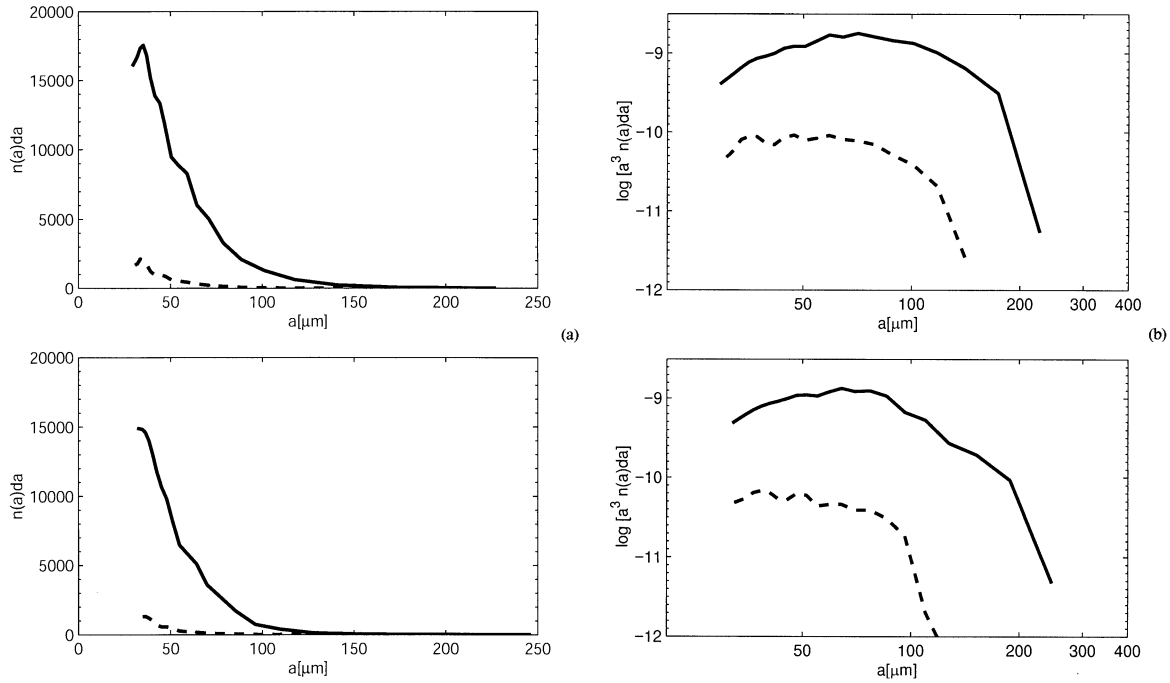

FIG. 3. Bubble size distributions at the center of 30 Langmuir bands at mean depths of (top) 2.1 and (bottom) 3.9 m and in wind speeds of 10.6 and 11.9 m s^{-1}, respectively. (a) The bubble number concentration, $n(a)da$ [the number of bubbles per cubic meter with radius a between $(a - 0.5)$ and $(a + 0.5)$ μm], averaged over the 30 Lc bands. The dashed line shows the mean bubble concentrations at 8 s before and after the center of the bands is reached. (b) $\log[a^3 n(a)da]$. Here $a^3 n(a)da$ is proportional to the void fraction per unit radius band and is averaged over values at the center of all 30 bands.

jected to increased hydrostatic pressure, and their buoyant rise through the water, factors identified by Garrettson (1973) as being important in describing bubble dynamics. Where models vary and where there remains considerable uncertainty are in the representation of the field of motion that disperses bubbles from their sources at the water surface (see section 5). Other areas of great uncertainty are the bubble size distribution generated by breakers and the frequency and energetics of breaking across the range of sizes of breaking waves. Several basic assumptions about bubbles and their surrounding turbulence [including some identified by Thorpe (1986)] underpin the validity of many models of bubble dynamics and their contribution to air–sea gas flux. These are reviewed in the following section in the light of the observations described in section 2.

4. The validity of assumptions in existing models of bubbles

The models referred to in section 3 generally assume that the following effects are negligible.

a. Fragmentation of bubbles

Models assume that bubbles are not shattered by turbulence and can be tracked as single particles. The radius of the smallest bubble, which may be broken up by turbulence, is given by the Hinze scale, $a_H = c(\gamma/\rho)^{3/5}\varepsilon^{-2/5}$, where c is a constant, γ is the surface tension, ρ is the density of the sea water, and ε is the rate of dissipation of turbulent kinetic energy per unit mass. Garrett et al. (2000) estimate c as 0.5, but Deane and Stokes (2002) suggest that this value is applicable in a steady state, such as a jet from a hosepipe entering the water, and that a value of about 0.83 (given by $2^{-8/5}$ times a critical Weber number of about 4.7 to the power 3/5) is more appropriate in the transient conditions of breakers. Extreme values, $\varepsilon_{\max}$, at $z/H_s = 2.22$ of about 3.2×10^{-5} m^2 s^{-3} (see Fig. 1) are 5.3 times the law of the wall value at this depth at the observed wind speed of 12.4 m s^{-1}. Taking $\gamma = 7.2 \times 10^{-2}$ N m^{-1} for "clean" and 3.6×10^{-2} N m^{-1} for a "dirty" bubble, one covered by an immovable surfactant film, respectively, $\varepsilon = \varepsilon_{\max}$, and $\rho = 1.03 \times 10^3$ kg m^{-3}, we find a_H is at least 0.1 m (clean bubbles) or 0.07 m (dirty bubbles), using the lower value $c = 0.5$ suggested by Garrett et al. These values of a_H are much larger than the vast majority of bubble radii observed or inferred at $z/H_s = 2.22$, even in the regions of bubble concentration in Langmuir bands. Turbulent fragmentation of large volumes of air trapped within spilling or plunging breakers is observed by Deane and Stokes within the high ε breaker regions at shallower depths but is not significant in the disruption of bubbles at the depths considered here.

b. Coalescence of bubbles

Models neglect coalescence that may reduce bubble numbers and lead to larger bubbles. Neglecting the differential rise of bubbles of different radii, the number of collisions per unit time and per unit volume between neutral particles of radii a_j and a_k of numbers per unit volume, n_j and n_k, respectively, in a turbulent fluid of viscosity ν is given by

$$N_{jk} = 1.3(\varepsilon/\nu)^{1/2}(a_j + a_k)^3 n_j n_k \quad (1)$$

(Saffman and Turner 1956). To obtain a rough estimate of the likelihood of a significant number of collisions, we take $a = a_j = a_k = 30$ μm representing the size at the peak in Fig. 3a and numbers of 10^5 m^{-3}, representative of bubbles with size between 30 and 130 μm, and extreme values $\varepsilon_{\max}$ and $v_{f\max}$. This gives $N_{jk} = 1.6 \times 10^{-3}$ collisions s^{-1} m^{-3}. The rise speed of bubbles in a quiescent ambient fluid, w_b, is about 0.4 and 0.2 cm s^{-1} for clean and dirty bubbles of 30-μm radii, respectively, are so that (disregarding dissolution and expansion as they rise and pressure reduces) their lifetimes before reaching the surface from $z = 1.93$ m are 482 s and 965 s, respectively. Supposing that the turbulence is locally sustained at the extreme values during the rise periods, an unlikely scenario, the number of collisions per bubble during these rise times are 7.7×10^{-6} and 1.5×10^{-5}, respectively. (These numbers become 2.5×10^{-5} and 5.7×10^{-5} if a value $a = 70$ μm is used to characterize the peak in the volume size distribution, Fig. 3b.) Even if all collisions led to bubble amalgamation, which is also unlikely, this would have at most a very small effect on the bubble size population, implying that turbulence-induced collisions are negligible. Thorpe (1986) shows that collisions caused by differential rise speeds are also negligible.

c. Distortion of bubbles from spherical shape by turbulence

This affects the rise speeds of the spherical bubbles assumed in the models. Turbulence will induce bubble oscillations that may affect their rise speeds as well as leading to sound generation (e.g., see Lamarre and Melville 1994). Significant distortion will occur if bubble radii are much greater than the smallest characteristic length scale of the turbulence, the Kolmogorov length scale, $l_k = (\nu^3/\varepsilon)^{1/4}$. Taking again the extreme value $\varepsilon_{\max}$ at $z/H_s = 2.22$, $l_k = 420$ μm, greater than the majority of bubble radii (Fig. 3a), and implying that at these depths the bubbles remain approximately spherical.

d. Effect of a cloud of bubbles on bubble rise speed

The mean speed of ascent of a layer of bubbles in a cloud differs from that of a single bubble. The mean rise speed is $w_b(1 - 6.55v_f)$ (Batchelor 1972) where w_b is the rise speed of a single spherical bubble in the absence of others. The correction, $6.55v_f$, is negligible for even the highest void fractions, $v_{f\max}$, observed at $z/H_s = 2.22$.

e. Interaction of bubbles and mean flow

These interactions are generally ignored in models. Although Smith (1998) has suggested that vacillations in the strength of Lc may be associated with the reduction in its downwelling by the buoyancy of high bubble concentrations, the maximum mean v_f observed in Lc is only about 1.6×10^{-7} at $z/H_s = 1.92$ and winds of about 10.6 m s^{-1} (Fig. 2b). While this void fraction is equivalent to the density change caused by a temperature variation of about 1 mK and variations of this size are typical of those found in Lc (Thorpe and Hall 1982; Thorpe et al. 2003), it leads to a drag per unit mass or a fluid acceleration, gv_f, of 1.6×10^{-6} m s^{-2}, very much less than that typically encountered by fluid downwelling in Lc cells of order $u_{\rm Lc}^2/l$ or about 10^{-3} m s^{-2} [where $u_{\rm Lc}$ is the maximum downwelling speed, typically $O(0.1$ m s$^{-1})$, and l is the depth to which the cell extends, typically 10 m]. At the respective depth bubbles appear to have negligible effect on Lc. In the immediate wake of breaking waves where bubble concentrations and void fractions are relatively high, holes appearing in patches of floating foam indicate that the momentum transport from rising bubbles to the water is, however, enough locally to generate substantial vertical motion (Thorpe et al. 1999).

f. Effects of turbulence on bubble rise speeds

These are generally disregarded in models of gas flux. The effect of turbulence is generally to impose lift and drag forces that reduce the rise speed of small bubbles by factors that depend on the ratio $\beta = u'/w_b$ and are sensitive to the energy spectrum function $E(k)$ of the turbulence, where u' is the root-mean-square vertical velocity of the turbulent velocity fluctuations and k is the wavenumber of the turbulent motion. In homogeneous and isotropic turbulence when $0 < \beta < 1$, Spelt and Biesheuvel (1997) show that the rise speed decreases with β, and may be reduced by a factor of 2–3 at $\beta = 1$, depending critically on the chosen representation of turbulence. Their numerical results suggest that at $\beta \sim 1$ the reduction in rise speeds is sometimes associated with the transient capture of bubbles in turbulent vortices, although this requires further investigation. Since u' is of order u_{*w}, the parameter β is of order u_{*w}/w_b. To estimate u_{*w} we assume that the stress at the water surface is approximately continuous so that $\rho_a u_*^2 = \rho u_{*w}^2$, where the ratio of the ratio of the density of air, ρ_a to that of water, ρ, is about 1.2×10^{-3}, and use

$$u_*^2 \approx C_D W_{10}^2 \quad (2)$$

to calculate the friction velocity in the air u_* with a drag coefficient chosen as

$$C_D = 10^{-3}[0.75 + 0.067W_{10}\ (\text{m s}^{-1})] \quad (3)$$

(Geernaert 1990). In the wind speeds of 10–12 m s^{-1} in which the observations described in section 2 are made, u_{*w} is (1.3–1.6) cm s^{-1}, and β is of order unity for bubbles with radii of about 70–90 μm, near the peak of the volume size distributions (Fig. 3b). In the upper ocean, however, turbulence is probably neither isotropic nor homogeneous. While the size of β suggests that turbulence is likely to reduce the bubble rise speeds, particularly where large dissipation rates accompany bubbles, the knowledge of the nature of turbulent motion [e.g., of $E(k)$ within the down-going flow in Lc] is insufficient to make any assessment of the magnitude of the reduction.

g. *Contribution of bubbles to the generation of turbulence*

Models assume that the bubbles react passively to turbulence and that turbulence is not generated by rising bubbles. Bubbles may contribute substantially to the motion field if the following situations occur:

i) They shed eddies with a scale and with vorticity comparable to those within the ambient *turbulence*, thereby contributing to the turbulent motion. Taking $a = 250$ μm and $w_b = 4.2$ cm s^{-2} for bubbles covered with surfactants which immobilize their surface, to characterize the largest (and few) observed bubbles and to give extreme values, the bubbles' Reynolds number Re is about 10 and the Weber number, We $= w_b(\rho a/\gamma)^{1/2}$, is 0.11. These values are much less than the critical values, Re = 202 and We = 1.26 at which bubbles begin to oscillate as they rise (Hartunian and Sears 1957). While flow may separate and form vortex rings which are stationary relative to the rising bubbles, they are unlikely to be shed or detached from the bubbles except possibly in the presence of impurities (e.g., microscopic particles) in the water. The scale of attached wake eddies is comparable to that of the bubble radii, a, and by section 4c, is consequently generally less than the Kolmogorov scale. Although Re is small, there may however be interactions between rising bubbles which may promote the detachment of bubble wake eddies or lead to random motions, which may contribute to turbulence. The vorticity of shed eddies is of order of the bubbles' rise speed, w_b, divided by a. This is about 170 s^{-1} for the scales considered, exceeding the vorticity in turbulent eddies of order $(\varepsilon/\nu)^{1/2} \approx 5.7$ s^{-1}. In view of the relatively rare close approach of bubbles (see section 4b), interactions are infrequent and the contribution of such eddies to turbulence appears negligible at the depths considered here.

ii) They are substantially distorted by the turbulent motion, consequently being a sink of turbulent energy (section 4c indicates this effect is insignificant).

h. *Effect of turbulence on gas transfer rates from single bubbles*

This affects dissolution rates assumed in models. It is negligible, provided

$$(\varepsilon/\nu)^{1/2} < O[(4g^2D/81\nu^2)^{1/3}], \quad (4)$$

where D is the diffusivity of the bubble's gas in the water and g is the acceleration due to gravity (Batchelor 1980). Taking the typical value, $D = 2 \times 10^{-9}$ m^2 s^{-1} and ε_{max} as before, (4) becomes 5.7 $s^{-1} < O(21.5$ $s^{-1})$, which is (just) satisfied.

A further assumption made in many models is that a *steady state* exists with a uniform distribution of sources. This is a more difficult assumption to justify, although waves appear to break randomly and not preferentially at a position of earlier breaking (Thorpe et al. 2003) and the location of breaking does not appear to be affected by windrows (Thorpe 1992). The assumption might be better avoided by devising models in which bubbles are injected from breakers that conform to observations (e.g., that have the same recurrence period at a point, that inject bubbles randomly into an underlying Lc pattern, and that produce bubbles at a rate representing those in real breakers at specified wind speeds).

The dependence of the calculations made above on the rate of turbulent dissipation emphasizes the need to obtain further measurements of dissipation rates and bubble size distribution, especially within the breaker zone closer than 1 significant wave height from the sea surface. Without such observations we are left with the option of constructing a model in which bubbles are injected at some specified level near the sea surface with atmospheric gas composition, but without representation of the uncertain factors described above.

5. K_z and Lc in models

Thorpe (1982) used the measured variation of acoustic scattering cross section with depth and wind speed to derive estimates of the flux of oxygen and its variation with gas saturation in the water. The estimates were revised by Thorpe (1984d). While this method does account, in principle, for the wide variations in bubble clouds caused by breakers by using real data to represent their natural variability, it cannot account for the variation of the gas composition within bubbles as gases pass at different rates from bubbles during their lifetimes. It is consequently flawed. Thorpe (1984a) therefore devised a turbulent diffusion model based on a Monte Carlo simulation of dispersion from a near-surface source of bubbles containing two gases, O_2 and N_2, injected into the sea at atmospheric concentrations. In the absence of reliable data to guide in the selection of better alternatives, the effective vertical diffusion coefficient of momentum, the eddy viscosity, was chosen to be constant. Available optical measurements of bub-

ble size distribution (Johnson and Cooke 1979) were used to constrain the models. It was assumed in some models (e.g., Thorpe 1982, 1984b, 1986), that the eddy diffusivity of bubbles was the same as that of momentum, that is, equal to eddy viscosity. As demonstrated in sections 8 and 9, this assumption is erroneous. (In the atmospheric literature it is usual to introduce a correction factor expressing the ratio of the two eddy diffusion coefficients.)

Models of a wide range of suspensions, including sediment over the seabed or blowing snow (e.g., Taylor et al. 2003), use an eddy-diffusion-based representation of turbulence. Results are in fairly good agreement with observations without a requirement for any specific representation of vortices or eddies in the flow. It may consequently appear sufficient to represent the dispersion of bubbles in the upper ocean using a bubble dispersion model based on a Monte Carlo method, perhaps constructed to give a law of the wall eddy viscosity, $K_z = ku_{*w}z$. This, however, fails to represent the presence of Lc and its known tendency to trap bubbles (Stommel 1949). The agreement between eddy diffusion models and observations for other suspensions may be because the flow field at the distances from the boundary, where comparison is made is not dominated by large eddies that contain a substantial concentration of suspended matter, or because the turbulent flow differs in its basic structure from that in the upper ocean. Langmuir circulation is generally thought to be generated and driven by the CL2 mechanism (e.g., see Leibovich 1983; Li and Garrett 1995), which depends on a vortex force resulting from the presence of shear flow and the Stokes drift induced by wind waves. This large eddy structure of the upper ocean may be absent in other boundary layer flows where the particular mechanisms forcing Lc are absent and where eddy diffusion based models are therefore more successful. It follows that, in modeling the dispersion of bubbles, some realistic representation is required of the nature of the vortical motions, the ''large eddies'' below the water surface that may contribute to bubble trapping or maintenance within the water column, particularly of coherent motions in which the largest downward flow is greater than the bubble rise speed, typically about 0.5–4 cm s^{-1}.

The advective effect of a single-cell-sized representation of Lc was included in a bubble diffusion model by Thorpe (1984c). This model was later used to investigate the effects of temperature, gas saturation, and particulate concentrations on bubble size distribution (Thorpe et al. 1992), and developed to include four gases and to investigate the effect of varying the velocity in Langmuir cells on gas transfer (Woolf and Thorpe 1991). It was subsequently used by Farmer et al. (1999) with a modified representation of the flow within the Langmuir cell to predict bubble size distributions for comparison with those measured using a bubble resonator. Gemmrich and Farmer (1999a) devised a model including a one-size-cell representation of Lc to explain their observations of near-surface temperature fluctuations in winds of 12–16 m s^{-1} and significant wave heights of about 4.5 m.

Simple examples of how the effective vertical diffusivity of bubbles is affected by Lc are given in section 8. Consideration is given to the combined effect of cells of different sizes in section 9.

In addition to the problem of appropriately representing Lc in models of gas transfer, there is a major problem of parameterizing turbulence and bubbles close to the sea surface where breaking waves are a critical component, both in injecting bubbles and in generating turbulence. Agrawal et al. (1992) and Terray et al. (1996) find that at depths, z, less than the significant wave height, H_s, the rates of dissipation of turbulent kinetic energy per unit mass, ε, exceed the law of the wall relationship, $\varepsilon = u_{*w}^3/kz$. Simultaneous measurements of bubbles and dissipation are not yet available within depths less than H_s, the region where the representation of diffusion is most uncertain and where, in or close to breaking waves, the bubble void fractions may be of the order 10%–60% (Lamarre and Melville 1991; Deane and Stokes 2002). The observations described in section 2 are also beyond this depth range.

6. The effect of Langmuir circulation on submerged bubbles

Langmuir circulation will be particularly effective in bubble transport when the depth to which bubbles are driven by breaking waves exceeds the depth at which the downwelling motions in Lc first exceed the rise speed typical of bubbles, w_b. In these conditions bubbles are advected downwards by the circulation and may be captured in a subsurface recirculating region. The discussion in section 2 suggests that the maximum depth to which turbulence and consequently bubbles are carried through the direct action of wave breaking is about $1.5H_s$. The largest downwelling motions observed by Weller et al. (1985) are typically 10–20 cm s^{-1} and occur near the middle of the mixed layer. Scaling of Lc speeds with wind or other velocity scales is poorly known. Smith (1999) finds a scaling of surface currents in Lc with Stokes drift, but with other presently unknown factors affecting the constant of proportionality. D'Asaro (2001) finds that the rms vertical speeds in the mixing layer (excluding those directly induced by waves) are some 1.75–2.0 times greater than those found in turbulent flow near a rigid wall, with maximum values of $1.41u_{*w}$ at depth of about 0.2 times the mixed layer depth. This appears to differ from Weller et al.'s finding of largest motions at middepth but may be a consequence of (i) vacillations in the strength or presence of Lc and processes associated with cell amalgamation or break down or (ii) a broadband scaling of Langmuir cells, leading to enhanced motions caused by the relatively small cells that affect mainly the shallower layers. We consider the effects of the latter in section 9.

To proceed further in making a rough, but quantitative, estimate of the possible effect of Lc on dispersion, we make the ad hoc assumptions that the downwelling speed varies sinusoidally in the vertical and that the maximum is equal to the surface convergence speeds, estimated to be

$$u_{\mathrm{Lc}} = (3.42 \times 10^{-3})W_{10} + 2.7 \times 10^{-3}, \qquad (5)$$

where W_{10} is the 10-m wind in units of meters per second and u_{Lc} also has units of meters per second. This is greater than D'Asaro's rms values. This is expected, the downwelling speeds in Lc being rather larger than the rms values. It is further assumed that the Langmuir cells are square with depth equal to the observed width,

$$l = 0.235W_{10} + 4.935, \qquad (6)$$

with units in meters. Equations (5) and (6) are based on observations in a deep lake for winds in the range $3 < W_{10}\ (\mathrm{m\ s^{-1}}) < 22$ and are taken from Thorpe et al. (1994). The downwelling speed in the cells is $u_{\mathrm{Lc}} \sin(\pi z/l)$. The depth at which the typical rise speed is equal to the downwelling speed is

$$z_{\mathrm{Lc}} = (l/\pi) \sin^{-1}(w_b/u_{\mathrm{Lc}}). \qquad (7)$$

The ratio, R, of the depth to which bubbles are transported on injection by breakers to that at which their rise speed is equal to the downwelling speed in Lc is about $1.5H_s/z_{\mathrm{Lc}}$. Taking an estimate for the significant wave height to be

$$H_s = 0.96(c^3u_*)^{1/2}/g \qquad (8)$$

(Csanady 2001), a wave age $c/u_* = 14$ (corresponding the the conditions of Figs. 1–3), and using (2) and (3), the ratio becomes

$$R = 0.237(0.75 + 0.067W_{10})W_{10}^2/gl \sin^{-1}(w_b/u_{\mathrm{Lc}}). \qquad (9)$$

The mean bubble radius at the peak of the mean volume size distribution near 70 μm appears to change only slowly with depth (Farmer et al. 1999). When the rise speeds of 70-μm bubbles, 0.9 cm $\mathrm{s^{-1}}$ (dirty) or 1.4 cm $\mathrm{s^{-1}}$ (clean), u_{Lc} from (5) and l from (6) are substituted into (9), we find that, for dirty bubbles, $R = 1$ when $W_{10} = 8.3$ m $\mathrm{s^{-1}}$ and, for clean bubbles, $R = 1$ at $W_{10} = 9.5$ m $\mathrm{s^{-1}}$. The observations appear to be just above the transition where Lc is becoming effective in bubble transport. At higher wind speeds the advective effect of Lc will have an even greater effect on vertical dispersion.

7. Modeling the effects of Lc

Two eddy diffusion coefficients are defined in the models that represent dispersion of bubbles or, as below, of particles with local concentration, $C(x, z, t)$, which has bubblelike properties. The first is K_z, the eddy viscosity, ascribed to momentum transport by small-scale turbulent motions, motions that are of scale much less than those of Lc and are uncorrelated to Lc. The second is the effective diffusivity K_p produced by the combined effects of small-scale turbulence and Lc. We assume here that turbulence is of much smaller scale than the Lc cells and that the two are independent, but stress that our observations showing enhanced turbulence in particular locations within Lc cells (e.g., Fig. 2) suggest that this assumption is not robust. Attention is focused on two questions:

1) How much does Lc change the effective vertical eddy diffusivity K_p?
2) What is the effect of multiple cells?

A model is adopted with steady flow independent of downwind direction y, in an x (across wind) and z (downward vertical) cellular circulation. (There is insufficient data to construct a more realistic model with vacillation or cell merger and break down.) The particles are introduced into a near-surface layer (see below). They rise at a uniform speed w_b, representing the buoyant rise of bubbles and decay exponentially in time immediately following release at a constant rate p, to represent bubble dissolution. (For simplicity, the effects of pressure in reducing bubble volume are not specifically represented. Nor are the effects of turbulence referred to in section 4f: information about their magnitude is lacking.) The numerical method follows that used by Thorpe (1984c) for constant eddy diffusivity K_z, tested by comparison with an analytical solution. Several parameters were used in the earlier model:

$$\theta = lu_{\mathrm{Lc}}/4\pi K_z, \qquad (10)$$

a measure of the relative effects of Lc and eddy diffusivity on particle diffusion;

$$\varphi = lw_b/4\pi K_z, \qquad (11)$$

measuring the relative importance of bubble rise and eddy diffusion; and

$$q = lp^{1/2}/2\pi K_z^{1/2}, \qquad (12)$$

measuring the relative importance of particle decay and eddy diffusion. Values of these parameters are given in tables below to allow comparison to be made. In the model the particle rise speed w_b is taken as 0.009 m $\mathrm{s^{-1}}$ to correspond to 70-μm-radius dirty bubbles and the model concentrations found may be representative only of this particular bubble size. The small-scale diffusivity K_z is represented by use of the standard Monte Carlo technique, and Lc is represented by the streamfunction

$$\psi(x, z) = -(lu_{\mathrm{Lc}}/\pi) \sin(x\pi/l) \sin(\pi z/l). \qquad (13)$$

with velocity components $\partial\psi/\partial z$ and $-\partial\psi/\partial x$, in the x (cross wind) and z (vertical) directions, independent of the downwind direction, y, and where u_{Lc} is given by (5). New particles are introduced at a mean rate Q_0 at each time step and at random positions within $0 < z < 1.5H_s$ and across the width $2l$ of two Langmuir cells having downward flow between them at position $x =$

0, with H_s given by (8) and l by (6). Particles reaching a location $z < 0$ after a time step are assumed to have surfaced. Particles below the cell depth l are subsequently moved only as a consequence of their rise speed and the eddy diffusivity. Two different K_z distributions were adopted: a value that does not vary in depth,

$$K_z = 2.6 \times 10^{-5} W_{10}^3/g, \quad (14)$$

used by Gemmrich and Farmer (1999a), and

$$K_z = ku_{*w}(1.5H_s) \quad \text{in } 0 < z < 1.5H_s \quad \text{or}$$
$$K_z = ku_{*w}z \quad \text{in } 1.5H_s < z, \quad (15)$$

corresponding to a law-of-the-wall distribution with enhanced values in the wave injection region.[2]

Thorpe (1982) shows that the decay rate, $p = (1/a)da/dt$, of dirty bubbles of radius a composed of O_2 and N_2 and at depth z in water that is 100% saturated in both gases, is given by

$$p = RTD\text{Nu}[\kappa_O q + \kappa_N(1 - q)]z/[a^2(z + H)], \quad (16)$$

provided $2\gamma/g\rho az \ll 1$, where R is the gas constant, T is the temperature in K, D is the (approximately equal) diffusivities of the two gases in seawater, Nu is the Nusselt number, κ_O and κ_N are the coefficients of absorption of O_2 and N_2, respectively, q is the mole fraction of O_2, and H is the water depth at which the pressure is twice atmospheric. If $a = 70$ μm, Nu $\approx 2\text{Pe}^{1/3}/\pi$, where Pe is the Peclet number (Pe $= aw_b/D$; see Thorpe 1982), and taking $H \approx 10$ m, $R = 8.31 \times 10^{-3}$ m^3 kPa K^{-1} mol^{-1}, $T = 283$ K, $\kappa_O = 0.49$ g m^{-3} kPa^{-1}, $\kappa_N = 0.21$ g m^{-3} kPa^{-1}, $D = 2 \times 10^{-9}$ m^2 s^{-1}, and $q = 0.215$ (equal to the atmospheric fraction—an approximation), we find at $z = 2$ m that $2\gamma/g\rho az = 5 \times 10^{-2}$ which is small, as required, and from (16), $p = 0.006$ 25 s^{-1}. This value of p is chosen to be representative of the bubble diffusion rates, for simplicity ignoring variations with depth and time.

The horizontally averaged concentration of particles, $\mathbf{C}(z, t)$, is determined at wind speeds of 6–14 m s^{-1}, after 96 particles of unit concentration have been added at each 1 s time step randomly across the domain width of depth $1.5H_s$ representing that within which bubbles are injected by breaking waves. The model was run until a steady state was reached, judged by steady concentration, $\mathbf{C}$, values and equality (to better than 10%) between the numbers of particles injected and those reaching the surface per time step. This required 800–2400 time steps, the latter in the higher winds. Values of u_{Lc}, H_s, and l at the wind speeds of 6–14 m s^{-1} of model runs are given in Table 1.

TABLE 1. Values of scales and parameters corresponding to the different wind speeds, W_{10}, examined in the numerical model. Five values of wind speed W_{10} are given, with corresponding Lc speeds u_{Lc} [see (5)], significant wave height H_s [see (8)], and cell depth l [see (6)]. The lifetime and concentrations are those of bubbles reaching the surface after release at random positions in the depth range $0 < z < 1.5$ H_s when there is no eddy diffusivity and no Lc.

W_{10} (m s^{-1})	u_{Lc} (cm s^{-1})	H_s (m)	l (m)	Lifetime (s)	Conc^n
6	2.32	0.21	6.35	17.2	0.894
8	3.10	0.42	6.82	35.0	0.810
10	3.65	0.73	7.28	60.8	0.700
12	4.37	1.15	7.76	95.8	0.583
14	5.06	1.69	8.23	141	0.470

The mean concentration $\mathbf{C}(z)$ is given by a diffusion equation

$$\frac{\partial \mathbf{C}}{\partial t} - w_b\frac{\partial \mathbf{C}}{\partial z} = \frac{\partial}{\partial z}\left[K_p(z)\frac{\partial \mathbf{C}}{\partial z}\right] - p\mathbf{C} + Q, \quad (17)$$

with z downward [see also Thorpe (1982, their (41) but with sign corrected] similar model equations are described by Thorpe 1984c,a]. Here $Q(z)$ is the rate of input of $\mathbf{C}$ per unit volume. In a steady state (17) can be written

$$d/dz[K_p(z)d\mathbf{C}/dz] = p\mathbf{C} - w_b d\mathbf{C}/dz - Q. \quad (18)$$

[Analytical solutions are possible[3] when particular forms are selected for p and K_p, for example when K_p is constant or $K_p = ku_*z$; Thorpe 1982, 1984c.] Once $\mathbf{C}$ is determined from the numerical model, (18) can be integrated to give the effective diffusion coefficient, $K_p(z)$:

[2] If the overall eddy viscosity within the near-surface region is given by a law of the wall formulation as suggested by the Autosub measurements of ε, it appears inappropriate to include *both* a formulation of eddy diffusivity in the form, $K_z = ku_{*w}z$, *and* a representation of momentum diffusion by Lc, within the same model. If however (as here) the motion within Lc is as represented by (13), steady and purely two-dimensional in the (x, z)-plane normal to the wind direction y, with no mean shear flow in the x direction, then the spatially averaged product of the two components of velocity induced by Lc, $\partial\psi/\partial z$ and $-\partial\psi/\partial x$, at a given depth will be zero. So too will products of the circulation velocity components with those of small-scale turbulent motions *provided the two are uncorrelated.* The contribution of Lc to the x-directed Reynolds stress momentum transfer is therefore zero unless the turbulent fluctuations are correlated to the circulatory flow field. (The high ε in the downwelling motion of Lc found in section 2 suggests this assumption of decorrelated Lc and turbulent motions is not valid.) It is usual to define an eddy diffusion coefficient as a stress divided by a mean velocity gradient, but in this case both stress and velocity shear are zero. There is no immediate route to estimating an overall eddy viscosity (other than K_z) in the present two-dimensional model.

[3] An analytical solution of (18) without Lc but with particle rise and decay, with K_p = constant and with injection of the quantity at a constant rate, Q_0, in $0 < z/H_s < 1.5$, satisfying the condition of zero flux as z tends to infinity, and continuity of $\mathbf{C}$ and of its vertical flux at $z = 1.5H_s$, is

$$\mathbf{C}(z) = \begin{cases} (Q_0/p)\{1 - [q_-/(q_+ - q_-)]\exp[q_-(1.5H_s - d)] \\ \qquad + B\exp(q_-z)\} \quad \text{if } 0 < z < 1.5H_s, \quad \text{and} \\ (Q_0/p)\{[q_+/(q_+ - q_-)]\exp[q_-(z - 1.5H_s)] \\ \qquad + B\exp(q_-z)\} \quad \text{if } z > 1.5H_s, \end{cases}$$

where $q_\pm = [-w_b \pm (w_b^2 + 4pK_z)^{1/2}]/2K_z$ and B is a constant, determined by, say, a surface value of $\mathbf{C}$.

$$K_p(z) = \left\{K_z(0)\left(\frac{d\mathbf{C}}{dz}\right)_0 + \int_0^z p\mathbf{C}\, dz - w_b[\mathbf{C} - \mathbf{C}(0)] - \int_0^z Q\, dz\right\} \Big/ \left(\frac{d\mathbf{C}}{dz}\right), \quad (19)$$

where $(d\mathbf{C}/dz)_0$ is the concentration gradient at the surface $z = 0$ and the integral (numerically a summation) is taken from $z = 0$ to depth z. At the surface where there is no vertical component of motion induced by Lc, $K_p = K_z$. The values of $\mathbf{C}$ found in the numerical diffusion model by averaging over many particles between depth z and $z + dz$ can be used in (19) to find $K_p(z)$ once a steady state is reached.

A second estimate of the particle diffusion coefficient, K_p, is obtained from the equation defining the downward flux of particles across a constant depth plane:

$$K_p = -A_v[Cw]/(d\mathbf{C}/dz), \quad (20)$$

where $A_v[\ ]$ is the mean value at depth z and w is the downward component of particle speed due to the combination of random diffusive walk, Lc, and rise. Tests with $u_{\mathrm{Lc}} = 0$ show that values of K_p determined using (19) tend to be lower than K_z if $z/H_s > 2.5$, and less rapidly convergent and more scattered than values of K_p determined using (20). The latter is therefore used to determine values of the diffusivity ratio,

$$r = K_p/K_z. \quad (21)$$

We can also estimate the effective diffusion coefficient, K_{Lc}, due to the Lc alone:

$$K_{\mathrm{Lc}} = -A_v[Cw_{\mathrm{Lc}}]/(d\mathbf{C}/dz), \quad (22)$$

where $w_{\mathrm{Lc}} = -\partial\psi/\partial x$ is the downward component of particle speed due to Lc. The ratio of K_{Lc} to K_p, is

$$s = A_v[Cw_{\mathrm{Lc}}]/A_v[Cw], \quad (23)$$

which provides a measure of the relative contribution of the flow in the Langmuir cells to vertical diffusion of particles.

8. Model results: Single cells

Figure 4 shows results when K_z is given by (14). The full lines show steady-state values of $\log\mathbf{C}$ as a function of z/l at various wind speeds with (full line) u_{Lc} set to zero (i.e., without Lc) and (crosses) with u_{Lc} given by (5). The bottom of the particle injection region is marked by an arrow. Below this the solutions for $\mathbf{C}$ without Lc decay exponentially. A similar decay is seen at depths below the bottom of the Langmuir cells at $z/l = 1$. The main effect of the circulation is to increase the concentration below the injection region and to produce a region near the center of the cell where the concentration is uniform or increases with depth leading to negative particle diffusivity, K_p. In consequence, values of r in this region are large or negative. (Negative values where the concentration gradient becomes positive are not shown in Fig. 4.) For comparison, Fig. 5 shows similar plots when K_z is given by (15). The concentration is again enhanced by the circulation but decays gradually in runs with or without Lc; as in observations and in contrast to Fig. 4, no uniform concentration layer is found. The location of the foot of the Langmuir cell is not evident in the concentration profiles, and the maximum values of r are typically about 2, much lower than in Fig. 4.

Tables 2 and 3 give parameter values and model estimates of the mean times for which injected particles take to reach the surface (the particle lifetimes), the standard deviation of these times Σ_t, and the mean concentrations of particles reaching the surface, once a steady state is established. Corresponding values with no eddy diffusivity and no Lc, only particle rise, are given in Table 1. Lifetimes are increased and concentrations decreased with the addition of Lc. Lifetimes increase with increasing wind speed, with a commensurate decrease in the concentrations. The relative values with and without Lc provide an indication of the effect of Lc in retaining submerged bubbles and so providing longer periods of time for gas diffusion to occur. When $W_{10} \geq 8$ m s^1, values of Σ_t exceed the mean bubble lifetimes, indicative of a pdf that is positively skewed, many particles surfacing rapidly after introduction but a number being submerged for relatively long periods by Lc. The ratio of Σ_t to the mean bubble lifetimes is greatest (about 1.5) at $W_{10} \approx 8$ m s^{-1}, close to the value where Lc begins to subduct injected bubbles (section 6). There is no substantial difference in the variation of the ratio, s, for the two forms of K_z examined, nor significant variation with W_{10}. In each case s exceeds unity over the major extent of the cell depth, with values of typically 2.5 at middepth, indicating the strong influence, but not overwhelming domination, of the circulation in driving the vertical transport of particles. Values of θ in Table 2 (K_z uniform in depth) are large, inferring that Lc dominates over eddy diffusivity, while φ and q decrease, but are of order unity, implying the particle rise and decay are important in comparison with eddy diffusion (but still less so than Lc). Parameters θ (proportional to u_{Lc}/u_{*w}) and q shown in Table 3 are calculated for values of K_z given by (15) at the center of the cell, $K_z = ku_{*w}l/2$. Values of θ are of order unity, so here eddy diffusion, Lc, and particle decay are of comparable importance, but φ (proportional to w_b/u_{*w} and a measure of particle rise) is relatively small.

Model runs in which the depth of injection of particles was halved show similar trends but with concentrations at depths $l/2$ reduced by a factor slightly more than 2, and with a reduction in the mean particle lifetimes.

9. Model results: Multiple cells

So far, effects of the so-called observed hierarchy of cell sizes have been ignored in modeling or only in-

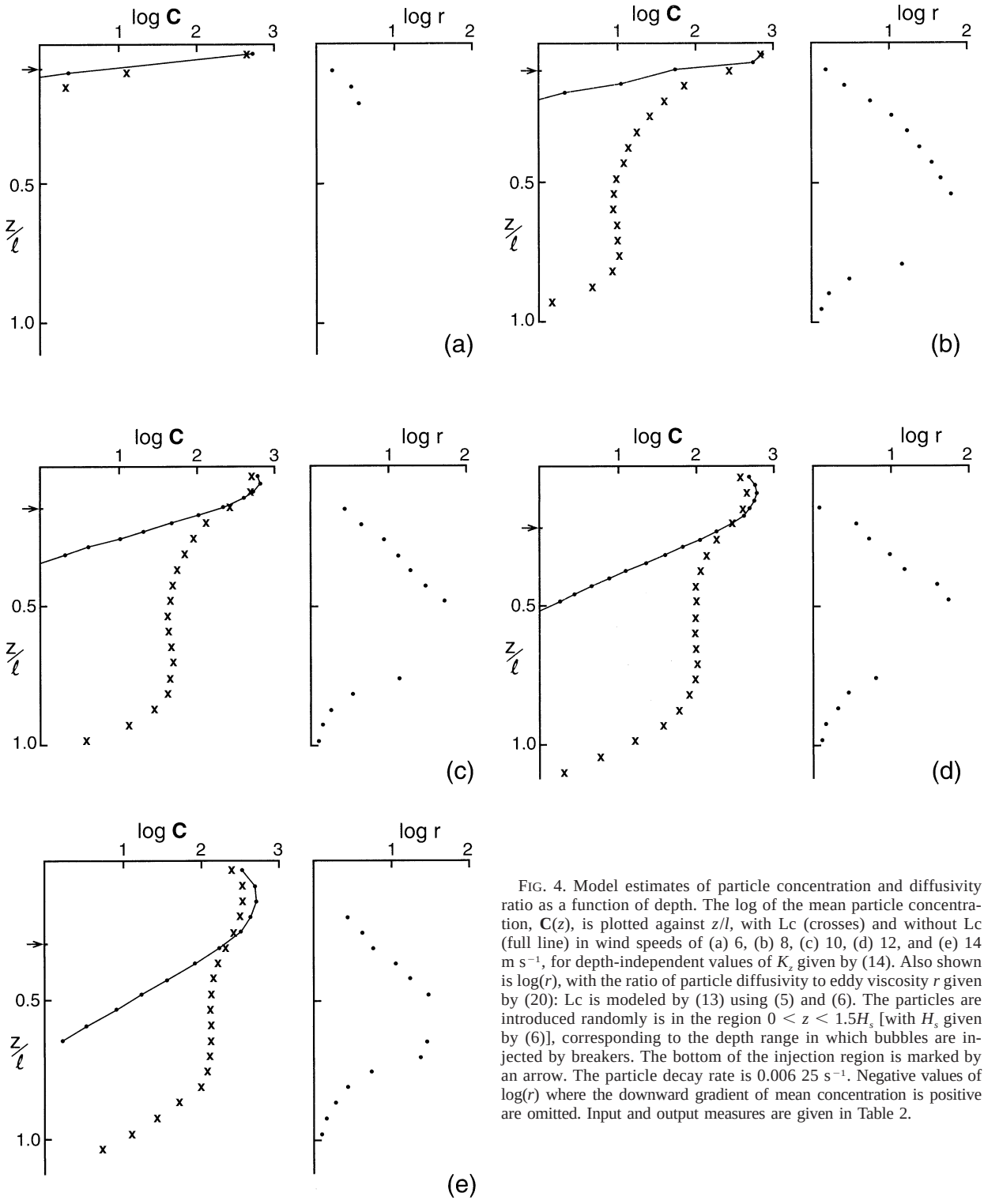

FIG. 4. Model estimates of particle concentration and diffusivity ratio as a function of depth. The log of the mean particle concentration, **C**(z), is plotted against z/l, with Lc (crosses) and without Lc (full line) in wind speeds of (a) 6, (b) 8, (c) 10, (d) 12, and (e) 14 m s^{-1}, for depth-independent values of K_z given by (14). Also shown is log(r), with the ratio of particle diffusivity to eddy viscosity r given by (20): Lc is modeled by (13) using (5) and (6). The particles are introduced randomly is in the region $0 < z < 1.5H_s$ [with H_s given by (6)], corresponding to the depth range in which bubbles are injected by breakers. The bottom of the injection region is marked by an arrow. The particle decay rate is 0.006 25 s^{-1}. Negative values of log(r) where the downward gradient of mean concentration is positive are omitted. Input and output measures are given in Table 2.

cluded, by inference, within the effects of eddy diffusivity. Estimation of the effect of smaller cells requires quantitative information about how their vertical velocities and penetration depths relate to their horizontal size. These sizes appear to have a lognormal distribution, symptomatic of turbulence (Csanady 1994). The smaller cells may

i) enhance the diffusivity in the near-surface layer;
ii) augment the downward velocities in larger cells if

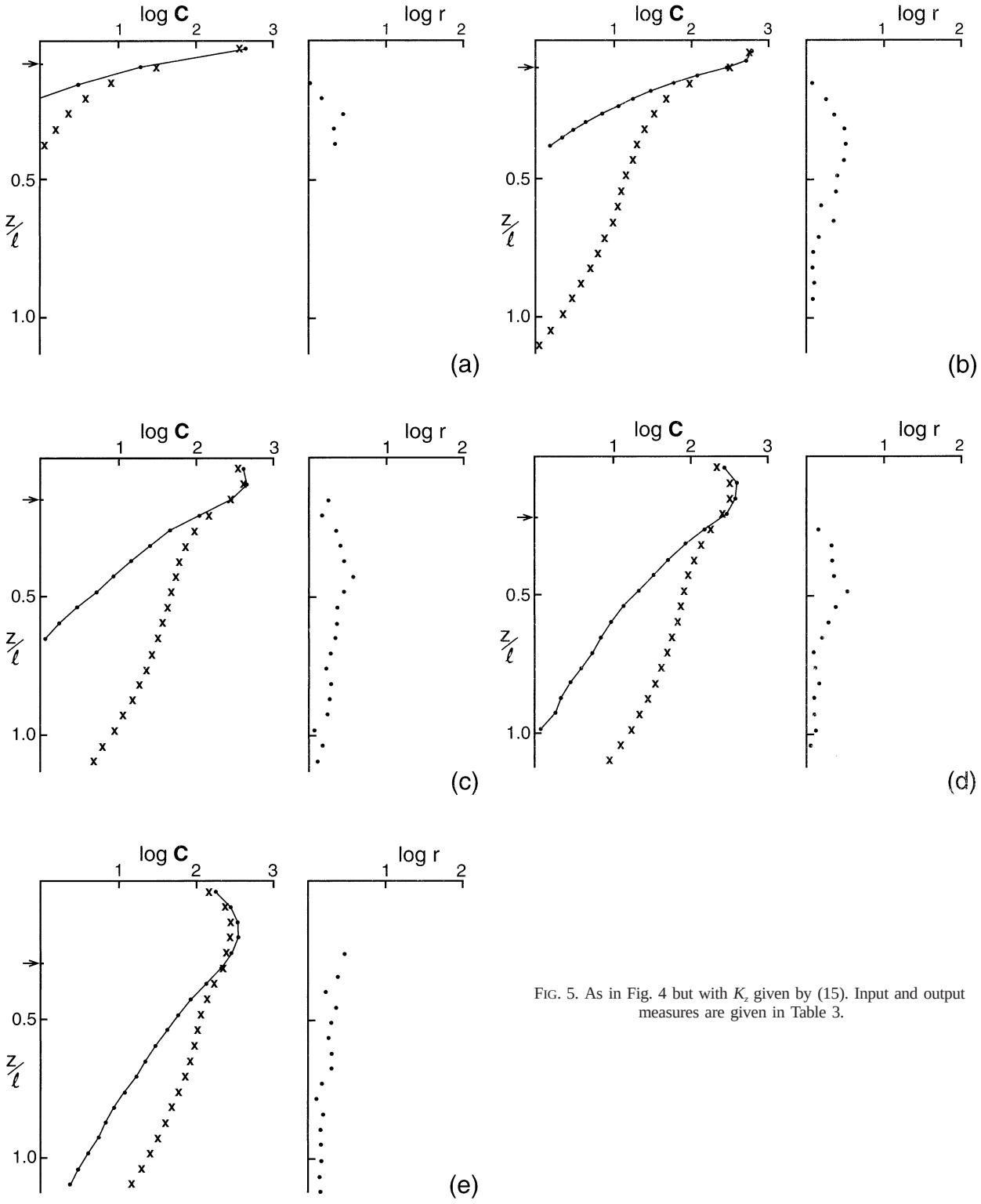

FIG. 5. As in Fig. 4 but with K_z given by (15). Input and output measures are given in Table 3.

they are coincident in position, so reducing the depths at which the downward speed equals the rise speeds of bubbles in the larger cells, or advect bubbles to depths at which the vertical velocities in large cells exceeds bubble rise speeds, so effectively increasing the parameter R characterizing the effectiveness of cells in vertical transport; or

iii) reduce the vertical rise speeds of bubbles as they,

TABLE 2. Values corresponding to the profiles in Fig. 4 with K_z given by (14), independent of z. Values u_{Lc}, H_s and l [see (6)] are as given in Table 1. Here Σ_t is the std dev of the bubble lifetimes. The two values of lifetime Σ_t and concentration are those of particles reaching the surface with no Lc/with Lc. Values of θ, φ, and q are found from (10)–(12) and of R from (9).

W_{10} (m s^{-1})	K_z (m^2 s^{-1})	Lifetime (s)	Σ_t (s)	Conc^n	θ	φ	q	R
6	5.72×10^{-4}	70/71	35/47	0.662/0.660	20.5	7.94	3.33	0.126
8	1.36×10^{-3}	88/120	50/184	0.603/0.586	12.0	3.59	2.33	0.305
10	2.65×10^{-3}	114/220	78/323	0.538/0.501	8.07	1.97	1.78	0.608
12	4.58×10^{-3}	152/355	125/438	0.470/0.405	5.89	1.21	1.44	1.07
14	5.84×10^{-3}	177/400	178/422	0.409/0.345	4.55	0.81	1.21	1.73

and the smaller cells, are advected toward downwelling regions in larger cells, so enhancing the number of bubbles supplied to the deeper downwelling region of larger cells.

It is also conceivable that the small cells or vortices generated by breakers are bodily subducted by much larger cells, so contributing to subsurface turbulence, but this is not investigated here.

The effect of multiple cell sizes has been examined by including in the model

i) nonoverlapping cells with scales l and $l/2$ and speeds u_{Lc} and $u_{Lc}/2$, respectively, but with the same total number of bubbles as in the single cell case (this is equivalent to there being twice as many cells of half scale);
ii) superimposed cells of scales l and $l/2$ with speeds u_{Lc} and $u_{Lc}/2$, respectively [in this case the downward flows of both cells are located at the same position, so enhancing the local downward flow (this is equivalent to conditions in which the smaller cells are advected into the convergence regions of the larger cells)]; or
iii) nonoverlapping cells with scales $5l/6$, $3l/4$, and $l/2$ with speeds $5u_{Lc}/6$, $3u_{Lc}/4$, and $u_{Lc}/2$, respectively, close to those of the primary cell, l and u_{Lc}, but with the same total number of bubbles as in the single cell case [model runs (i) and (ii) were also made with third sets of nonoverlapping or superimposed cells of size and speed equal to one-third of the largest].

Results for wind speeds of 10 m s^{-1} are shown in Figs. 6 and 7 for K_z given by (14) and (15), and with supporting data given in Tables 4 and 5, respectively. The addition of more nonoverlapping cells, as in (i) above (Figs. 6a, 7a), leads to relatively fewer particles being carried by Lc to depth, reducing the concentration and ratio, r. The superposition of cells, as in (b) above (Figs. 6b, 7b), strengthens the downwelling and more particles are transported downwards, enhancing the concentration and r, particularly at depth $z < l/2$, where ratios approaching 10 are found. Addition of the third cells makes relatively little difference. For the depth-uniform eddy diffusion coefficients (Fig. 6), the thickness of the region of near-uniform or inverted concentration is increased, but the ''law of the wall'' profiles of K_z (Fig. 7) have concentrations that decay more nearly exponentially with depth. Nonoverlapping cells slightly reduce bubble lifetimes and their standard deviation Σ_t (Tables 4 and 5), while superimposed cells increase lifetimes and Σ_t, and reduce the concentration of surfacing particles, implying an enhancement of the gas flux.

For comparison, Fig. 8 shows the results of including nonoverlapping cells of similar sizes as in (iii) in winds of 10 m s^{-1}, with corresponding lifetimes and concentrations given in Table 6. The effect is to removed the depth-range of near-uniform mean concentration and of very high r when K_z is uniform in depth and to produce a concentration profile similar to that of a law of the wall eddy diffusivity. Values of s reach 1.5 for K_z given by (15), lower than those of 2.3 when K_z is given by (14).

10. Discussion

a. Model assumptions tested against observations

Concurrent observations of ε and v_f near the sea surface are presented in section 2 and are used in section

TABLE 3. Values corresponding to the profiles in Fig. 5 with K_z given by (15) and calculated at $z = 1.5H_s$. Values u_{Lc}, H_s, and l [see (6)] are as given in Table 1. Here Σ_t is the std dev of the bubble lifetimes. The two values of lifetime, Σ_t and concentration are mean values for particles reaching the surface with no Lc/with Lc. Values of θ, φ, and q found from (10)–(12) are calculated using the value of K_z at mid–cell depth ($z = l/2$). Values of u_{Lc}, H_s, l, and R are as given in Table 1.

W_{10}/u_{*w} (m s^{-1})	K_z (m^2 s^{-1})	Lifetime (s)	Σ_t (s)	Conc^n	θ	φ	q
6/0.007	8.9×10^{-4}	70/74	38/66	0.663/0.660	1.31	0.229	0.842
8/0.010	2.49×10^{-3}	89/119	63/177	0.608/0.592	1.18	0.145	0.729
10/0.013	3.20×10^{-3}	115/172	106/249	0.555/0.533	1.10	0.109	0.655
12/0.016	11.32×10^{-3}	143/212	147/291	0.510/0.488	1.04	0.087	0.604
14/0.020	20.18×10^{-3}	167/214	172/266	0.475/0.467	0.99	0.072	0.565

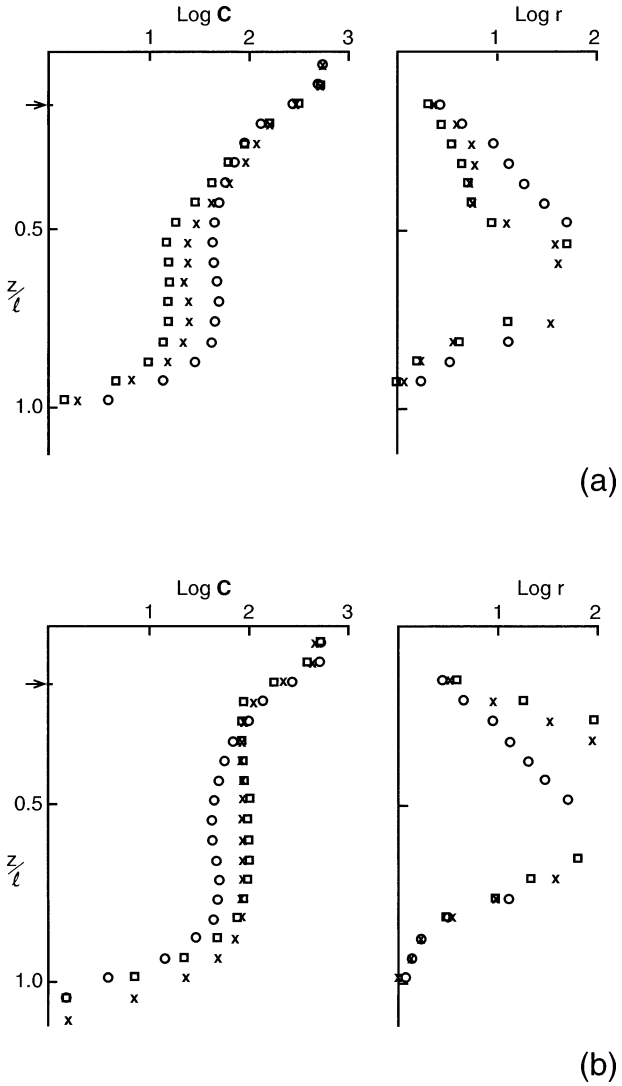

FIG. 6. Particle concentration and diffusivity ratio r vs z/l with K_z given by (14) for (circles) 1 cell, (crosses) 2 cells, and (squares) 3 cells. The wind speed is 10 m s^{-1} and ancillary values are given in Table 4. Negative values of log(r) where the downward gradient of mean concentration is positive are omitted. (a) Nonoverlapping cells; (b) superimposed cells.

4 to test the assumptions commonly made in models of subsurface bubbles. In the wind speeds and wave conditions of the observations, these appear to be valid at depths greater than about $1.5H_s$. It is however important to note that, even at this depth some of the assumptions are only weakly satisfied and that *all* these assumptions may, and some clearly will, be violated in a more intense turbulence region described by Agrawal et al. (1992) and Terray et al. (1996) at depths less than $1.5H_s$. This is especially so in the proximity of breaking waves where enhanced turbulence will fragment bubbles, lead to collisions and perhaps coalescence, distort the bubbles leading to changes in rise speeds through the water and affect the rates of dissolution. Models designed to describe bubble gas flux in the immediate vicinity of breakers will have to account more carefully for the effects of turbulence on bubble dispersion, of large rising bubbles in producing turbulence, as well as other properties mentioned above, than does the present generation of models.

b. Langmuir circulation and algae

As well as leading to accumulation of bubbles, Lc causes increased concentrations of mobile or buoyant algae (e.g., see Bainbridge 1957; Smayda and Reynolds 2001). Turbulence affects the supply of nutrients to algae, may increase predator–prey contact and causes damage to flagellates (for review see Estrada and Berdalet 1998). For example, the growth of the red-tide dinoflagellate, *Genyaulex polyedra* Stein, is found to be inhibited when the turbulent shear, $S = (\varepsilon/\nu)^{1/2}$, is greater than about 3 s^{-1} (Thomas and Gibson 1990), although a much lower threshold may apply when turbulence is intermittent (Gibson and Thomas 1995). Turbulent shear has a negative effect on nitrogenase activity (NA) and CO_2 fixation by *Nodularia* strains of cyanobacteria at values of $S > 2.2$ s^{-1} (Moisander et al. 2002). Extreme values of $\varepsilon = 3.2 \times 10^{-5}$ m^2 s^{-3} (Fig. 1) at $z/H_s = 2.22$ give $S = 5.6$ s^{-1}, exceeding these thresholds, although mean values of ε give s = 1.6. Turbulence at the same depth in the Langmuir bands where motile or buoyant algae accumulate gives $S = 2.4$ s^{-1}, suggesting that some limitation of plankton growth will occur, given the variability of the circulation and turbulence. At shallower depths, the direct effects of breaking waves

TABLE 4. Values corresponding to the profiles for multiple cells in Fig. 6 with K_z given by (14) at $W_{10} = 10$ m s^{-1}; Σ_t is the std dev of the bubble lifetimes. The mean lifetimes may be compared with that of 60.8 s with no eddy diffusivity or Lc (Table 1). Values of u_{Lc}, H_s and l are as given in Table 1 and R as in Table 3 at 10 m s^{-1}.

No. of cells	Mean bubble lifetime (s)	Σ_t (s)	Mean bubble conc	Comments
1	220	323	0.501	
2	213	299	0.492	Nonoverlapping cells
3	191	260	0.497	Nonoverlapping cells
2	256	359	0.480	Superimposed cells
3	260	359	0.479	Superimposed cells

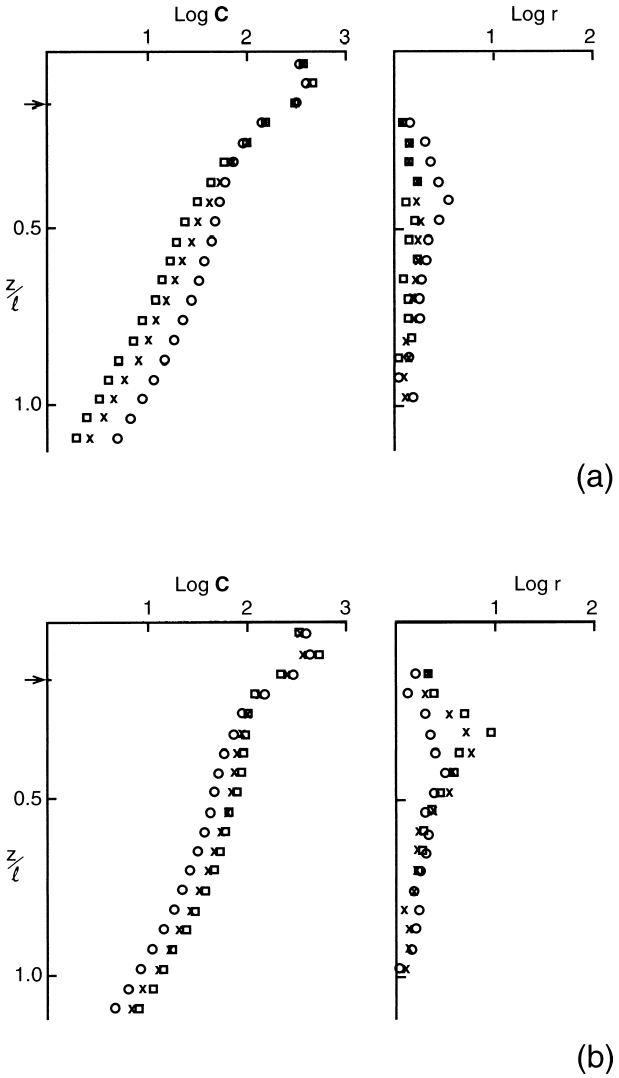

FIG. 7. Particle concentration and diffusivity ratio r vs z/l as in Fig. 6, but with K_z given by (15) for (circles) 1 cell, (crosses) 2 cells, and (squares) 3 cells. The wind speed is 10 m s^{-1} and ancillary values are given in Table 5.

become significant and turbulence is known to exceed the law of the wall variation. The nonuniform distribution of turbulence and algae needs to be considered in the construction of models of algal dynamics.

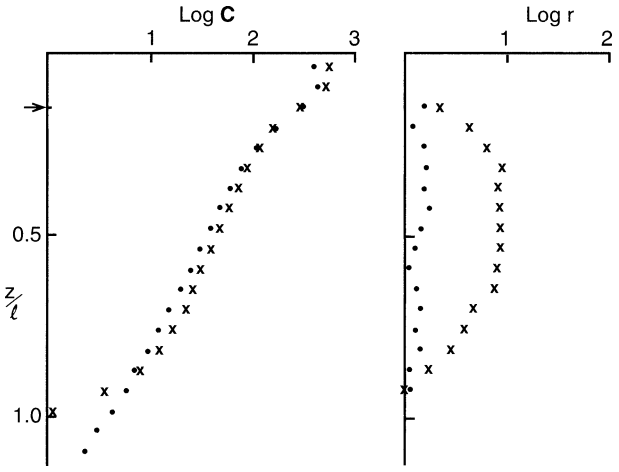

FIG. 8. Particle concentration and diffusivity ratio r vs z/l with K_z given by (14) (crosses) or (15) (dots) for the set of four nonoverlapping cells described by (iii) in text. The wind speed is 10 m s^{-1} and ancillary values are given in Table 6.

c. The effective diffusivity and mushroom clouds

Substantial increase in **C** occurs at mid–cell depth when the wind reaches about 8 m s^{-1} (see Figs. 4b, 5b). As seen by comparing **C** at $z/l = 0.5$ in Figs. 4c–e and 5c–e at winds of 10–14 m s^{-1}, the concentrations level off as the wind increases from 10 to 14 m s^{-1}, perhaps reaching ''saturation'' as the effects of Lc dominate the process of vertical transfer The largest increase in concentration occurs near the wind speeds that are in general accord with the condition, $R = 1$, in section 6 at which bubbles are injected to levels where vertical advection overcomes their tendency to rise. This simplistic estimate is however strictly valid only when K_z is negligible and takes no account of the downward vertical diffusion of particles as they are being advected by Lc towards the center of the downwelling region. The concentration profiles with no Lc (full lines in Figs. 4 and 5) show the effect of this diffusion may be substantial.

The concentration profiles with K_z given by (14) show increasing levels below the middepth of the cells (Figs. 4 and 6). This is a consequence of the vertical acceleration and deceleration of particles in Lc, a ''log jam'' effect occurring in horizontally averaged concentration profiles below middepth and resulting in negative K_p

TABLE 5. Values at $W_{10} = 10$ m s^{-1} corresponding to the profiles for multiple cells in Fig. 7 with K_z given by (15) at $z = 1.5H_s$; Σ_t is the std dev of the bubble lifetimes. The mean lifetimes may be compared with that of 60.8 s with no eddy diffusivity or Lc (Table 1). Values of u_{Lc}, H_s, and l are as given in Table 1 and R as in Table 3 at $W_{10} = 10$ m s^{-1}.

No. of cells	Mean bubble lifetime (s)	Σ_t (s)	Mean bubble conc	Comments
1	172	249	0.533	
2	159	215	0.530	Nonoverlapping cells
3	147	189	0.535	Nonoverlapping cells
2	189	267	0.523	Superimposed cells
3	184	259	0.525	Superimposed cells

TABLE 6. Values corresponding to the profiles for a combination of four nonoverlapping cells in Fig. 8 at $W_{10} = 10$ m s^{-1}; Σ_t is the std dev of the bubble lifetimes. Values of u_{Lc}, H_s and l are as given in Table 1.

K_z	Mean bubble lifetime (s)	Σ_t (s)	Mean bubble conc
Eq. (14)	222	315	0.490
Eq. (15)	169	232	0.526

values in (22). The deceleration in vertical motion occurs where the Lc streamlines diverge to produce a horizontal spread of relatively young advected particles, resulting in an ''inverted mushroom'' shape of concentration contours. Such inverted mushroom-shaped bubble clouds are sometimes seen in sonograph observations using narrow vertically pointing acoustic beams, notably in conditions when convection is favored (e.g., see Thorpe 1982, Figs. 11c and 13b,c). The greater local eddy diffusivity when K_z has a law-of-the-wall behavior spreads the downwelling jet and the particle concentration contours do not show the mushroom shapes.

The estimated values of the ratio, $r = K_p/K_z$, is not unity, as sometimes supposed, but depends on depth, z, and on the form selected for K_z. When K_z is independent of depth, values of r exceeding 10 or which are negative are found in the center of the cells where the vertical gradient in concentration becomes small or positive. In contrast, when the law of the wall variation of K_z is used, r is typically between 1 and 2, similar to values reported in the literature for sedimenting particles (e.g., see Taylor et al. 2003), and the mean concentration profiles have distributions that do not differ greatly from exponential, in general agreement with observations. The lifetimes of particles (Tables 2 and 3) also depends on the choice of K_z. The simple model shows that prediction of bubble distributions and of gas transfer (which is related to bubble lifetime) is sensitive to the selection of K_z and that a constant value will not give realistic results if cells of only one size are represented.

d. The hierarchy of cell sizes

One assumption common in models of the role of bubble in air–sea gas flux is that Lc can be represented by a regular array of cells of a single specified size (e.g., Thorpe 1982, 1984c; Woolf and Thorpe 1991; Farmer et al. 1999). Neither the hierarchy of cells that are known to occur simultaneously nor the random unstable nature of the circulation are included. The sensitivity of concentration profiles and hence gas transfer to the representation of Lc, in particular to the histogram of cell size and flow speeds, is demonstrated in section 9. The model runs (Figs. 6 and 7) show that the concentration profiles and diffusion ratios depend on the way in which cells coexist, whether small and large cells occur separately on the water surface, or whether they are superimposed. If small cells are generated by breaking waves within a preexisting larger cells [e.g., through the mechanism suggested by Csanady (1994)], then their effect may be to make the bubble concentration gradients more uniform (Fig. 7b), to enhance the eddy diffusion of bubbles, and to increase the bubble lifetimes (Table 4) and consequently the air–sea gas flux. The results are however sensitive to the range of cell sizes which are included. Figure 8 suggests that in a suitable combination of cells and flow speeds, even with K_z constant (or even zero), it may be possible to reproduce results similar to those with a law-of-the-wall K_z dependence.

e. Requirements for future models

LES models (Skyllingstad and Denbo 1995; McWilliams et al. 1997; McWilliams and Sullivan 2000) provide realistic representations of many aspects of Lc, allowing for three-dimensional effects, the unsteady turbulent nature of the circulation, and the development of cells of different size, and they may well prove suitable for future studies of the effect of bubble on air–sea gas flux. They do not at present, however, include a representation of breaking waves, or of their consequent bubble generation and production of vorticity and turbulence (McWilliams and Sullivan 2000). Recent developments of large wave simulations (LWS: see Dimas and Fialkowski 2000) may make the modeling of wave breaking and turbulence and bubble generation feasible in the future. Even if this becomes possible, it will be necessary to have more quantitative information about waves (their frequency of breaking and the bubbles and turbulence which they generate) and about Langmuir cells (particularly of their flow speeds, growth, persistence, and demise and of how, in reality, a hierarchy of cells of different scales is constituted) to tune and test dynamical models to a stage at which they can be regarded as being sufficiently reliable for accurate gas flux estimates or algal modeling. This is a challenging, multiple-parameter problem demanding multisensor observations in a variety of sea and wind states in which AUVs can play a useful part.

11. Summary

Concurrent observations of the rate of dissipation of turbulent kinetic energy and of the void fraction and size distribution of bubbles produced by breaking wind waves have been made using an AUV, Autosub, operating along constant depth ''legs'' near the sea surface. Regions of relatively high dissipation rates and high void fraction are observed in bubble bands produced by Lc. Data are used to test eight of the basic assumptions underpinning existing models of the subsurface distribution of bubbles and their effect on air–sea gas transfer. Where sufficient data is available, the assumptions appear to be generally valid at depths exceeding $1.5H_s$ and

in wind speeds of about 11.5 m s^{-1}, but may break down at shallow depths.

Langmuir circulation is known to lead to the concentration of mobile or buoyant algae, particularly in the downwelling regions, and the observed mean dissipation rates in these regions of the circulation are found to be close to those at which algal dynamics are significantly affected.

A simple model with parameters adjusted to those appropriate in the range $6 \leq W_{10}\,(\mathrm{m\,s^{-1}}) \leq 14$ is devised to examine the qualitative effect of Lc on the vertical diffusion of bubbles and the representation of Lc in models of gas diffusion. The circulation is particularly effective in vertical bubble transfer when bubbles are injected by breaking waves to depths at which they are carried downward by the circulation against their tendency to rise. The estimated values of the ratio r of the eddy diffusivity of particles (resembling bubbles) K_p to the eddy viscosity K_z depends on depth z and on the form selected for K_z. With Langmuir cells of a single size and when K_z is independent of depth, values of r that exceed 10 are estimated as the depth is approached at which the downwelling speed in the cells is greatest and where the mean vertical concentration gradient is small. Negative values of K_p, and therefore of r, occur at mid cell depths where the vertical gradient in particle concentration is positive even though K_z is positive. In contrast, when the law of the wall variation of K_z is used, values of r are typically between 1 and 2, and the mean concentration profiles have distributions which do not differ greatly from an exponential decay in depth, in general agreement with observations. The effect of nonoverlapping or superimposed Langmuir cells of different size is also investigated, and it is shown that their effects may be quite different. Multiple nonoverlapping cells of similar scales with K_z independent of depth can result in concentration profiles that resemble those of a law of the wall K_z. The periods of time for which particles remain submerged is increased by Lc and depends on the choice of K_v. The simple model therefore suggests that model prediction of bubble distributions and of gas transfer (which is related to bubble submergence time) is sensitive to K_z and to the size distribution of Langmuir cells.

The paper draws attention to several aspects of upper ocean dynamics for which data are not yet sufficient to construct realistic and quantitative models of transfer processes involving Lc. Many of the assumptions made in models of bubble clouds and their contribution to the air–sea transfer of gases depend on the rate of turbulent dissipation, and this emphasizes the need to obtain further measurements of dissipation rates and bubble size distribution, particularly at depths less than H_s.

Acknowledgments. The authors are grateful for the help provided by Jeff Jackson in programming and in the analysis of sonar and turbulence data and Peter Chandler in the analysis of the bubble resonator data, and thank the Autosub Team and master and crew of the *Tershelling*, without whose enthusiastic assistance the data would not have been obtained. Part of this research was undertaken with funding from NERC Grant NER/A/S/2000/00359. TRO was supported by the Office of Naval Research (Grant N000149910088). SAT thanks Prof. Alan Elliot (SOS, University College of North Wales, United Kingdom) for the use of a workstation, and Kate Davis for assistance with figures.

REFERENCES

Agrawal, Y. C., E. A. Terray, M. A. Donelan, P. A. Hwang, A. J. Williams III, W. M. Drennan, K. K. Kahma, and S. A. Kitagorodskii, 1992: Enhanced dissipation of turbulent kinetic energy beneath surface waves. *Nature,* **359,** 219–220.

Bainbridge, R., 1957: The size, shape and density of marine phytoplankton concentrations. *Cambridge Philos. Soc. Biol. Rev.*, 91–115.

Batchelor, G. K., 1972: Sedimentation in a dilute dispersion of spheres. *J. Fluid Mech.,* **52,** 245–268.

——, 1980: Mass transfer from small particles suspended in turbulent flow. *J. Fluid Mech.,* **98,** 609–623.

Csanady, G. T., 1994: Vortex pair model of Langmuir circulation. *J. Mar. Res.,* **52,** 559–581.

——, 2001: *Air–Sea Interaction.* Cambridge University Press, 239 pp.

D'Asaro, E. A., 2001: Turbulent vertical kinetic energy in the ocean mixed layer. *J. Phys. Oceanogr.*, **31,** 3530–3537.

Deane, G. B., and M. D. Stokes, 2002: Scale dependence of bubble creation mechanisms in breaking waves. *Nature,* **418,** 839–844.

Dimas, A. A., and L. T. Fialkowski, 2000: Large-wave simulation (LWS) of free-surface flows developing weak spilling breaking waves. *J. Comput. Phys.*, **159,** 172–196.

Estrada, M., and E. Berdalet, 1998: Effects of turbulence on phytoplankton. *Physiological Ecology of Harmful Algal Blooms*, D. M. Anderson et al., Eds., NATO ASI Series, Vol. G41, Springer, 601–618.

Farmer, D. M., and D. D. Lemon, 1984: The influence of bubbles on ambient noise in the ocean at high wind speeds. *J. Phys. Oceanogr.,* **14,** 1762–1778.

——, and M. Li, 1995: Patterns of bubble clouds organized by Langmuir circulation. *J. Phys. Oceanogr.,* **25,** 1425–1440.

——, and J. R. Gemmrich, 1996: Measurements of temperature fluctuations in breaking surface waves. *J. Phys. Oceanogr.,* **26,** 816–825.

——, S. Vagle, and A. D. Booth, 1998: A free-flooding acoustical resonator for measurement of bubble size distributions. *J. Atmos. Oceanic Technol.,* **15,** 1132–1146.

——, ——, and M. Li, 1999: Wave breaking, turbulence and bubble distributions in the ocean surface layer. *The Wind-Driven Air–Sea Interface,* M. Banner, Ed., School of Mathematics, The University of New South Wales, 187–192.

Garcia, H. E., and R. F. Keeling, 2001: On the global oxygen anomaly and air–sea flux. *J. Geophys. Res.,* **106,** 31 155–31 166.

Garrett, C., M. Li, and D. M. Farmer, 2000: The connection between bubble size and energy dissipation rates in the upper ocean. *J. Phys. Oceanogr.,* **30,** 2163–2171.

Garrettson, G. A., 1973: Bubble transport theory with application to the upper ocean. *J. Fluid Mech.,* **59,** 187–206.

Geernaert, G. L., 1990: Bulk parametrization for the wind speed and heat fluxes. *Surface Waves and Fluxes,* G. L. Geernaert and W. J. Plant, Eds., Vol. 1, Kluwer Academic, 91–172.

Gemmrich, J. R., and D. M. Farmer, 1999a: Near-surface turbulence and thermal structure in a wind-driven sea. *J. Phys. Oceanogr.,* **29,** 480–499.

——, and ——, 1999b: Observations of the scale and occurrence of breaking surface waves. *J. Phys. Oceanogr.,* **29,** 2595–2606.

Gibson, C. H., and W. H. Thomas, 1995: Effects of turbulence intermittency on growth inhibition of a red tide dinoflagellate *Gonyaulax polyedra* Stein. *J. Geophys. Res.,* **100,** 24 841–24 846.

Hartunian, R. A., and W. R. Sears, 1957: On the instability of small gas bubbles moving uniformly in various liquids. *J. Fluid Mech.,* **3,** 27–47.

Johnson, B. D., and R. C. Cooke, 1979: Bubble populations and spectra in coastal waters: A photographic approach. *J. Geophys. Res.,* **84,** 3761–3766.

Lamarre, E., and W. K. Melville, 1991: Air entrainment and dissipation in breaking waves. *Nature,* **351,** 469–472.

——, and ——, 1994: Void-fraction measurements and sound-speed fields in bubble plumes generated by breaking waves. *J. Acoust. Soc. Amer.,* **95,** 1317–1329.

Leibovich, S., 1983: The form and dynamics of Langmuir circulation. *Annu. Rev. Fluid Mech.,* **87,** 119–123.

Li, M., and C. Garrett, 1995: Is Langmuir circulation driven by surface waves or surface cooling? *J. Phys. Oceanogr.,* **25,** 64–76.

McWilliams, J. C., and P. P. Sullivan, 2000: Vertical mixing by Langmuir circulations. *Spill Sci. Technol. Bull.,* **6,** 225–238.

——, ——, and C.-H. Moeng, 1997: Langmuir turbulence in the ocean. *J. Fluid Mech.,* **334,** 31–58.

Melville, W. K., F. Veron, and C. J. White, 2002: The velocity field under breaking waves: Coherent structures and turbulence. *J. Fluid Mech.,* **454,** 203–234.

Moisander, P. H., J. L. Henck, K. Kononen, and H. W. Paerl, 2002: Small-scale shear effects on heterocystous cyanobacteria. *Limnol. Oceanogr.,* **47,** 108–119.

Rapp, R. J., and W. K. Melville, 1990: Laboratory measurement of deep-water breaking waves. *Philos. Trans. Roy. Soc. London,* **331A,** 735–800.

Saffman, P. G., and J. S. Turner, 1956: On the collision of drops in turbulent clouds. *J. Fluid Mech.,* **1,** 16–30.

Schudlich, R., and S. Emerson, 1996: Gas supersaturation in the surface ocean: The roles of heat, gas exchange and bubbles. *Deep-Sea Res.,* **43,** 569–589.

Skyllingstad, E. D., and D. W. Denbo, 1995: An ocean large-eddy simulation of Langmuir circulations and convection in the surface mixed layer. *J. Geophys. Res.,* **100,** 8501–8522.

Smayda, T. J., and C. S. Reynolds, 2001: Community assembly in marine phytoplankton: applications of recent models to harmful dinoflagellate blooms. *J. Plankton Res.,* **23,** 447–461.

Smith, J. A., 1998: Evolution of Langmuir circulation during a storm. *J. Geophys. Res.,* **103,** 12 649–12 668.

——, 1999: Observations of wind, waves and the mixed layer: The scaling of surface motion. *The Wind-Driven Air–Sea Interface,* M. Banner, Ed., School of Mathematics, The University of New South Wales, 231–238.

Spelt, P. D. M., and A. Biesheuvel, 1997: On the motion of gas bubbles in homogeneous isotropic turbulence. *J. Fluid Mech.,* **336,** 221–244.

Stommel, H., 1949: Trajectories of small bodies sinking slowly through convection cells. *J. Mar. Res.,* **8,** 24–29.

Stramski, D., and J. Tegowski, 2001: Effects of intermittent entrainment of air bubbles by breaking wind waves on ocean reflectance and underwater light field. *J. Geophys. Res.,* **106,** 31 345–31 360.

Taylor, P. A., P. Y. Li, and J. D. Wilson, 2003: Lagrangian simulation of suspended particles in the neutrally stratified surface boundary layer. *J. Geophys Res.,* in press.

Terray, E. A., M. A. Donelan, Y. C. Agrawal, W. M. Drennen, K. K. Kahma, A. J. Williams III, P. A. Hwang, and S. A. Kitagorodskii, 1996: Estimates of kinetic energy dissipation under breaking waves. *J. Phys. Oceanogr.,* **26,** 792–807.

Terrill, E. J., W. K. Melville, and D. Stramski, 2001: Bubble entrainment by breaking waves and their influence on optical scattering in the upper ocean. *J. Geophys. Res.,* **106,** 16 815–16 824.

Thomas, W. H., and C. H. Gibson, 1990: Quantified small-scale turbulence inhibits a red tide dinoflagellate *Gonyaulax polyedra* Stein. *Deep-Sea Res.,* **37,** 1583–1593.

Thorpe, S. A., 1982: On the clouds of bubbles formed by breaking wind-waves in deep water, and their role in air–sea gas transfer. *Philos. Trans. Roy. Soc. London,* **304A,** 155–210.

——, 1984a: A model of the turbulent diffusion of bubbles below the sea surface. *J. Phys. Oceanogr.,* **14,** 841–854.

——, 1984b: On the determination of K_v in the near-surface ocean from acoustic measurements of bubbles. *J. Phys. Oceanogr.,* **14,** 855–863.

——, 1984c: The effect of Langmuir circulation on the distribution of submerged bubbles caused by breaking waves. *J. Fluid Mech.,* **142,** 151–170.

——, 1984d: The role of bubbles produced by breaking waves in super-saturating the near-surface ocean mixing layer with oxygen. *Ann. Geophys.,* **2,** 53–56.

——, 1986: Bubble clouds: A review of their detection by sonar, of related models, and of how K_v may be determined. *Oceanic Whitecaps,* E. C. Monahan and G. MacNioaill, Eds., D. Reidel, 57–68.

——, 1992: Bubble clouds and the dynamics of the upper ocean. *Quart. J. Roy. Meteor. Soc.,* **118,** 1–22.

——, and A. J. Hall, 1982: Observations of the thermal structure of Langmuir circulation. *J. Fluid Mech.,* **114,** 237–250.

——, and ——, 1983: The characteristics of breaking waves, bubble clouds and near-surface currents observed using side-scan sonar. *Cont. Shelf Res.,* **1,** 353–384.

——, P. Bowyer, and D. K. Woolf, 1992: Some factors affecting the size distributions of oceanic bubbles. *J. Phys. Oceanogr.,* **22,** 382–389.

——, M. S. Curé, A. Graham, and A. J. Hall, 1994: Sonar observations of Langmuir circulation, and estimation of dispersion of floating bodies. *J. Atmos. Oceanic Technol.,* **11,** 1273–1294.

——, W. A. M. Nimmo Smith, A. Graham, and A. M. Thurnherr, 1999: Patterns in foam and shallow tidal flows. *The Wind-Driven Air–Sea Interface.* M. Banner, Ed., School of Mathematics, The University of New South Wales, 257–264.

——, T. R. Osborn, J. E. F. Jackson, A. J. Hall, and R. G. Lueck, 2003: Measurements of turbulence in the upper-ocean mixing layer using Autosub. *J. Phys. Oceanogr.,* **33,** 122–145.

Weller, R. A., J. P. Dean, J. Marra, J. F. Price, E. A. Francis, and D. C. Broadman, 1985: Three-dimensional flow in the upper ocean. *Science,* **227,** 1552–1556.

Woolf, D. K., and S. A. Thorpe, 1991: Bubbles and the air–sea exchange of gases in near-saturation conditions. *J. Mar. Res.,* **49,** 435–466.

Zedel, L., and D. M. Farmer, 1991: Organized structures in subsurface bubble clouds: Langmuir circulation in the open ocean. *J. Geophys. Res.,* **96,** 8889–8900.